LHCb-PUB-2022-003
February 3, 2023

Occupancy studies for the LHCb Run4 Mighty Tracker

Timothy Hume[1], Violaine Bellée[2], Olaf Steinkamp[2].

[1] *ETH Zurich, Zurich, Switzerland*
[2] *Physik-Institut, Universität Zürich, Zürich, Switzerland*

Abstract

Occupancy studies are reported for the downstream tracking stations in which the effects of secondary particle production in detector materials are considered. A simplified model of the material description for the Inner Tracker (IT) silicon pixel detector proposed for LHCb LS3 enhancements has been developed in GEANT4 to facilitate this study. The sources of secondary particles have been identified to characterise the contribution of various sub-detectors to the occupancy in the scintillating fibres (SciFi) of the downstream tracking stations. The impact of the IT material on occupancy is examined for two material descriptions: with and without DCDC converters. Two possible modifications of the SciFi to accommodate the IT are also compared. Simulated event samples have been produced for each detector geometry scenario, as well as for the current Upgrade I configuration.

1 Introduction

The LHCb experiment seeks to undertake new measurements with unprecedented precision in its search for new physics in CP-violating phenomena and rare decays in flavour physics, by operating at increased instantaneous luminosity to achieve higher data collection rates [1]. The wide physics programme of the LHCb experiment also aims at taking full advantage of the capabilities of a forward acceptance detector to undergo precise measurements in forward and high-p_{T} physics, as well as spectroscopy.

The LHCb detector is currently undergoing its first major Upgrade (Upgrade I) [2] in order to record data from proton-proton collisions at higher rates during LHC Run 3 and Run 4. The Upgrade I detector is designed to operate at an instantaneous luminosity of $2 \times 10^{33}\,\mathrm{cm}^{-2}\,\mathrm{s}^{-1}$, five times higher than the original detector. An important part of the Upgrade I detector is the SciFi tracker located downstream of the spectrometer magnet. The SciFi tracker consists of three planar tracking stations with four detection layers each. The active area of the detection layers is made of mats of 250 μm thin scintillating fibres oriented vertically in two of the four detection layers and with a small stereo angle in the other two.

A second major upgrade (Upgrade II) has been proposed by the LHCb collaboration in a Framework Technical Design Report [3], to be able to cope with an instantaneous luminosity of about $1.5 \times 10^{34}\,\mathrm{cm}^{-2}\,\mathrm{s}^{-1}$ starting from LHC Run 5. The proposed layout of the Upgrade II detector is illustrated in Fig. 1, along with the coordinate system which will be used throughout this document.

The LHCb coordinate system is a right-handed cartesian coordinate system that has its origin at the nominal pp interaction point. The z axis is oriented along the LHC beam axis, from the origin towards the muon stations [4]. The y axis points upwards and the x axis points outside of the LHC rings.

Amongst other changes, the Upgrade II detector will include a new tracking system. The three tracking stations downstream of the spectrometer magnet will consist of an inner (IT) and middle (MT) region made out of silicon pixel detectors and an outer region covered by scintillating fibres (SciFi). The detector is referred to as the Mighty Tracker. A possible layout of the Mighty Tracker detector is shown in Fig. 2.

It has also been suggested by the collaboration to make use of the long shutdown (LS3) between Run 3 and Run 4 for a smaller upgrade of the detector, referred to as LS3 enhancements. The enhanced detector would operate in Run 4 at the same instantaneous luminosity as in Run 3. In LS3 enhancements, a version of the Mighty Tracker comprising only the IT part of the silicon detector would be installed along with the outer detector made of scintillating fibres.

The layout of the tracking stations and the area to be covered by IT and MT is largely driven by the occupancies in the SciFi part of the Mighty Tracker stations.

In the present note, a simplified simulation of the geometry and material composition of IT layers has been added to the description of the SciFi in the Upgrade I detector in order to study the impact of the IT on the occupancy in the SciFi detector. The sensitive area of the SciFi detector has been modified to exclude the area covered by the IT. Several scenarios have been simulated for the passive materials of the IT and SciFi. Simulated

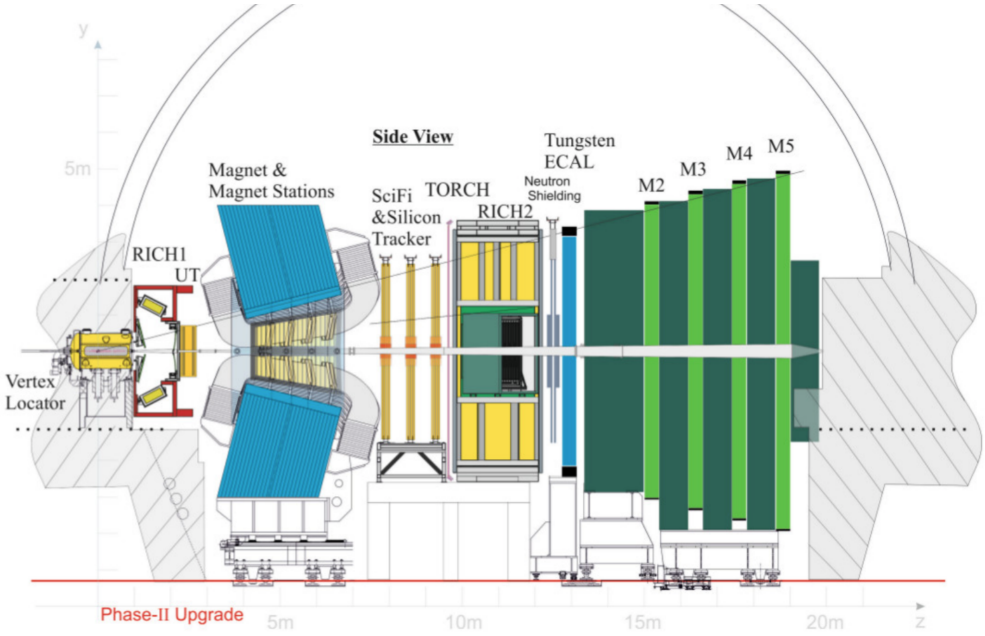

Figure 1: Schematic side-view of the Upgrade II detector and the y and z axes of its coordinate system.

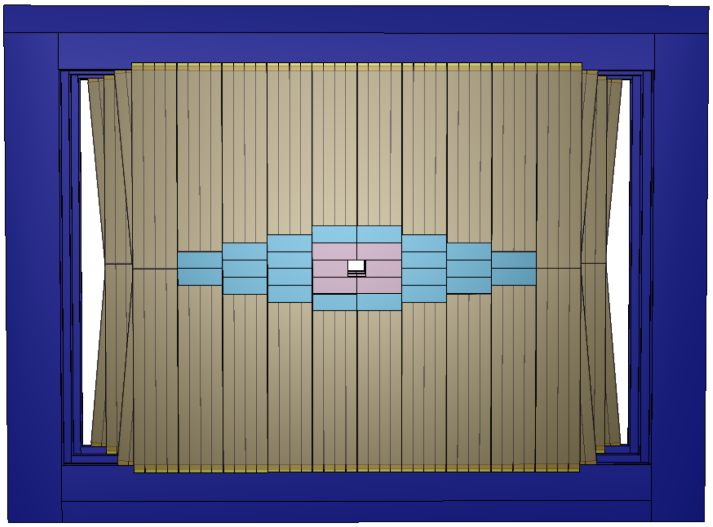

Figure 2: Possible layout of the Mighty Tracker detector in LHCb Upgrade II [3]. The region close to the beampipe is covered with silicon sensors (depicted in pink for the IT and in light blue for the MT). The outer region uses scintillating fibre technology (depicted in beige). Support structures outside of the LHCb acceptance are illustrated in dark blue.

events have been generated according to Run 4 beam conditions (corresponding to LS3 enhancements). The contribution of the several subdetectors to the occupancy in the downstream tracker has also been carefully studied by dividing the detector into regions corresponding to the main sub-detectors or groups of sub-detectors.

This note is organised as follows. After defining the various terms used throughout the document in Sec. 2, the different possible designs of the detector considered in this study

are described in detail in Sec. 3. The simulated data sets used for this work are listed in Sec. 4, as well as the associated software versions. In Sec. 5, the LHCb detector volume is separated into regions which are subsequently used in Sec. 8 to assess the origins of secondary particles detected by the Mighty Tracker. A brief study of the time and energy distributions of particle interactions in the detector material is shown in Sec. 6. The definition and methods for determining the occupancy in the SciFi tracker are outlined in Sec. 7. The breakdown of the occupancy according to contributions from secondary particles classified by their origin follows in Sec. 8. The differences between the various design options considered for the Mighty Tracker are reviewed in terms of occupancy in Sec. 9.Finally, conclusions are summarised in Sec. 10.

2 Nomenclature

For clarity, we define the following terms that are used throughout this note.

- **Region:** Slice of the LHCb detector volume defined by its limits in the z-direction (along the beam axis), intended to separate the main groups of sub-detectors of LHCb. Numbered from I to VI (from upstream to downstream).
- **Downstream tracker station:** Detector station incorporating one SciFi station and either one or two IT layers.
- **SciFi station:** Detector station made out of four SciFi layers (with fibres oriented along the x, u, v, and x directions) as well as their support structures, mirrors and cables. Numbered from 1 to 3 (from upstream to downstream).
- **SciFi layer:** Detector layer made out of one fibre layer and its associated passive material.
- **Fibre layer:** Active material of a SciFi layer, modelled as a single homogeneous block of material in the detector simulation.
- **Fibre x-layer:** Fibre layer with vertical fibres, i.e. measuring the x coordinate of the hits. There are two fibre x-layers per SciFi station, so six in the entire SciFi tracker, numbered here from 1 to 6 (from upstream to downstream).
- **Fibre:** Defined here as a 250 µm-wide section of a fibre layer. This definition of a fibre ignores the cylindrical shape of the real scintillating fibres and the fact that several layers of fibres are stacked together to form a fibre mat.
- **Fibre group:** Group of contiguous fibres along the horizontal direction perpendicular to the beam direction.
- **Mirrors:** Passive material due to light-weight mirrors glued to one end of the scintillating fibres.
- **IT station:** Detector station incorporating an IT layer and four IT cables.
- **IT layer:** Material inside the active area of the IT station, including silicon and passive material.

- **IT cable:** Copper cable running across the active area of the SciFi, needed to power one quarter of an IT layer.
- **DCDC converter:** If present, they make a significant contribution to the passive material of an IT layer. If not present, IT cables with larger cross section are required to power the IT.
- **Peak Fibres:** The groups of 80 fibres centred at positions $x = \pm 550\,\text{mm}$, including both the top ($y > 0$) and bottom ($y < 0$) fibre groups. These are the fibres just to either side of the area covered by the IT.
- **Central Fibres:** All fibres with x positions between the peak fibres (and excluding the latter). These are the fibres above and below the area covered by the IT.

3 Detector Description

The detector description used in this work is a modification of the reference Upgrade I detector description encoded in the software package GEANT4 [5, 6]. In Upgrade I, the design of the downstream tracking stations is entirely based on the scintillating fibre technology [7]. Each of the three tracking stations has four detection layers of scintillating fibres. The fibres extend from $y \approx 0$ upward and downward to the outer edges of the acceptance, where the light produced in the fibres is read out by Silicon Photomultiplier arrays (SiPMs). Fibres are arranged in 530 mm wide modules. The modules in the first and last layers of each station are vertical, while those in the two inner layers of each station are tilted by stereo angles of +5° and -5°, respectively. Modules above and below the LHC beampipe are modified to leave a 2×115.0 mm high and 2×130.8 mm wide rectangular hole around the beampipe. The material description of a SciFi layer inside the LHCb acceptance includes the material of the fibres and passive material of the detector modules. Additional material is present at the "inner" end of the modules, close to $y = 0$, due to light-weight mirrors that are glued to the ends of the fibres to help improve the light yield of the detector.

For the study presented here, the geometry of the Upgrade I SciFi Tracker as it is described in GEANT4 has been modified in order to include the IT stations in different configurations, as explained in Section 3.1. The mixture of materials introduced in the simulation to describe the different parts of the IT stations is discussed in Section 3.2.

3.1 Detector geometry

The geometry of the areas covered by IT and SciFi corresponds to the second of two LS3 enhancement options outlined in the occupancy study discussed in Ref. [8]. The IT covers a $2 \times 530\,\text{mm}$ wide and $3 \times 200\,\text{mm}$ high rectangular area, with a $200\,\text{mm} \times 200\,\text{mm}$ centred hole around the beampipe.

This active area includes the sensitive material (silicon) and passive materials (for structure, cooling, etc.). However, for this study the silicon implemented in the material of the IT layer in GEANT4 is only passive.

In addition to the material of the IT layer, the geometry description of the IT stations also includes four IT cables, which run across the active area of the SciFi and are modelled

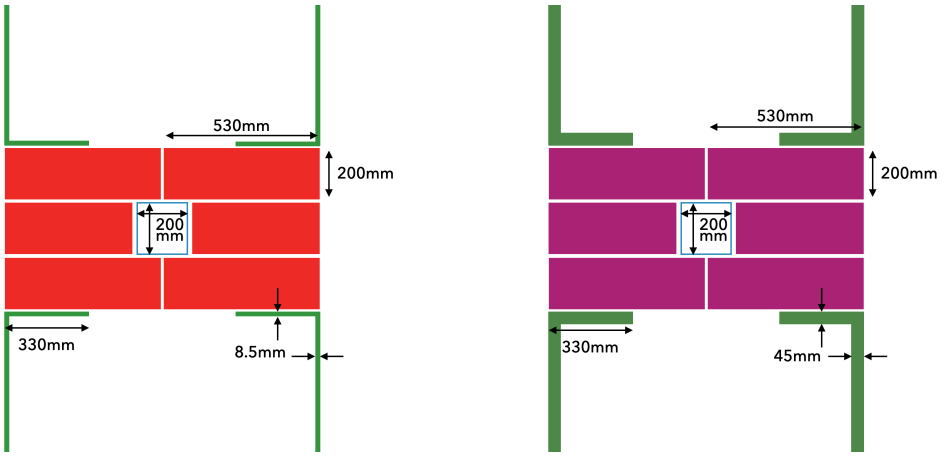

(a) With DCDC (b) Without DCDC

Figure 3: Schematic diagrams illustrating the geometries of one IT station in the two configurations studied. The IT layer composed of a composite material including DCDC converters are shown in red, while IT layers composed of a composite material without DCDC converters are in purple. The associated cables appear in green, and are wider when the IT surface does not include DCDC converters. Not drawn to scale.

by two rectangular volumes each, as illustrated in Fig. 3. Two different options are simulated:

- **With DCDC**: includes a contribution for DCDC converters in the description of the material budget inside the active area of the IT station and has narrower volumes describing the cables;
- **Without DCDC**: does not include a contribution for DCDC converters in the description of the material budget inside the active area of the IT station and has wider volumes describing the cables.

The numerical values of the geometry parameters for both options are summarised in Table 1.

Table 1: Parameters describing the geometry of the IT stations simulated in the two configurations.

Geometry parameter	Size (mm)	
	With DCDC	Without DCDC
IT layer width	1060	1060
IT layer height	600	600
Beam-pipe hole width	200	200
Beam-pipe hole height	200	200
IT layer thickness	29.9	29.3
Cable width	8.5	42.5
Cable thickness	1.0	1.0

The locations of the five IT stations along the z axis are illustrated in the schematic diagrams shown in Figure 4. Each of the IT stations has its centre 50 mm away from the

surface of the closest SciFi layer. Only five IT stations are implemented in the simulation due to the lack of space available between the last tracking station and the entrance window of the RICH2 sub-detector.

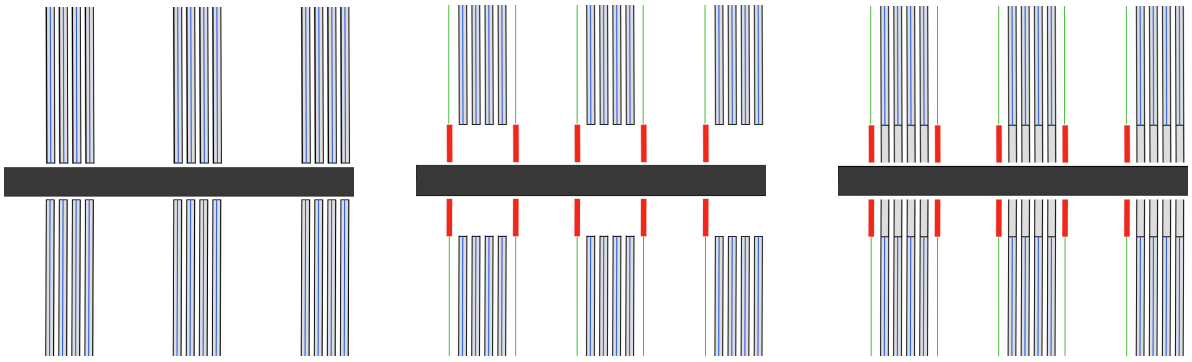

(a) Reference (b) Module Cut (c) Fibres Cut

Figure 4: Schematic diagrams illustrating different detector geometries studied. The SciFi layers are shown in grey, with enclosed fibre layers coloured blue. The thick black lines at the base of the fibres represent the mirrors. In (b) and (c), the IT layers are shown in red, IT cables appear in green. Not drawn to scale.

Three different options are simulated for the passive material of the SciFi, as illustrated in Figure 4:

- **Reference**: unchanged Upgrade I geometry (no IT volumes are added in this option);
- **Module cut**: the volumes describing the SciFi layers above and below the IT layers are shortened to exclude the area covered by the IT layers, the volumes describing the material of the mirrors are shifted accordingly;
- **Fibres cut**: the volumes describing the fibre layers above and below the IT layers are shortened to exclude the area covered by the IT layers; the volumes describing the material of the mirrors are shifted accordingly, but the volumes describing the remaining passive material of the SciFi layers are unchanged from the Upgrade I geometry.

In the options "Module cut" and "Fibres cut", the relevant SciFi volumes are shortened such that there is a 1 mm wide overlap in the xy plane between the area covered by the IT layers and the area covered by the fibre layers. In all three scenarios, the geometry description of the active area covered by the SciFi is modified to exclude the area covered by the IT. Note that occupancies are studied here only in the six x-layers of the SciFi. The numerical values of relevant geometry parameters for all three options are summarised in Table 2.

Table 2: Parameters describing the geometry of the SciFi stations simulated in the three configurations.

Geometry parameter	Size (mm)		
	Reference	Module cut	Fibres cut
Beampipe hole half width	130.8	529.0	130.8
Beampipe hole half height	115.0	299.0	115.0
Fibre length at $\|x\| < 130\,\text{mm}$	2309.0	2125.0	2125.0
Fibre length at $130 < \|x\| < 299\,\text{mm}$	2424.0	2125.0	2125.0
Vertical shift of mirrors at $\|x\| < 130\,\text{mm}$	115.0	299.0	299.0
Vertical shift of mirrors at $130 < \|x\| < 299\,\text{mm}$	0.0	299.0	299.0

Combining different options for IT and SciFi, the following four options for the description of detector material in the downstream tracking stations are studied:

- Reference (SciFi material as in Upgrade I, no IT), shown in Figures 7(a) and 7(c).
- Module cut (with DCDC), shown in Figures 7(b) and 7(d).
- Fibres cut (with DCDC), shown in Figures 8(a) and 8(c).
- Fibres cut (without DCDC), shown in Figures 8(b) and 8(d).

3.2 IT material

The material of the IT layers is modelled by a uniform mix of materials, obtained by estimating contributions from different detector elements. Variations in material composition within the IT layers are neglected. In order to make it realistic in terms of radiation length, the detector material is defined in simulation as a mixture of materials of given properties (chemical composition, density, radiation length) weighted by their respective mass fraction in the final material.

A list of the detector components considered in the simulation and their assumed material properties is given in Table 3. More details on the implementation of the materials in the LHCb software are given in Appendix F. For each detector component considered, an "effective thickness" is calculated from the assumed thickness of the detector component and the geometric fill factor of this component with respect to the surface of the IT layer. For example, cooling tubes are assumed to be 50 µm thick but covering only 12 % of the surface of an IT module, so their effective thickness is 6 µm.

The assumed material composition for the option "without DCDC" is based on studies documented in Ref. [3]. It includes contributions for silicon as sensitive material, PCBs and flex tape to treat and transport signals, carbon foam, carbon sheet, glue and Armacell for the mechanical structure and thermal insulation, as well as cooling tubes.

For the option "with DCDC", additional contributions from the material of DCDC converters are considered, taking into account copper coils, aluminium shielding and carrier PCBs. These contributions are calculated using estimates of the material composition of the DCDC converters from pictures and layouts in Ref. [9] and the expected number of DCDC converters required for powering one IT layer from Ref. [10].

The IT cables are described by a 1 mm thick layer of copper, corresponding to $X/X_0 = 7.1\%$.

Table 3: List of materials used in the mixture of materials that describes the IT layers, along with their properties as implemented in the simulation framework.

Material	Effective thickness (μm)	Layers	X_0 (cm)	Average X/X_0 (%)	Density (g/ cm^3)
Silicon	120	1	9.4	0.128	2.33
Cooling tube	6	2	28.6	0.004	1.42
Carbon foam	3200	1	185.7	0.172	0.20
Carbon sheet	300	2	23.7	0.253	1.72
Flex tape	340	1	9.6	0.356	1.71
Glue	120	1	35.5	0.033	1.30
PCB	314	1	17.0	0.185	2.44
Armacell	12300	2	801.3	0.307	0.08
Total without DCDC				**1.438**	
DCDC (copper)	103	1	1.4	0.720	8.96
DCDC (aluminium)	143	1	8.9	0.161	2.70
DCDC (PCB)	342	1	17.0	0.201	1.80
DCDC (total)				1.064	
Total with DCDC				**2.502**	

3.3 Scans of radiation length and interaction length

The radiation length fraction, X/X_0, of the mix of material described in the previous section is an input to the geometry description, whereas the interaction length fraction, λ/λ_0, is computed in GEANT4 based on the chemical composition of the various materials. In order to validate the material and the geometry description, scans of radiation length and interaction length have been performed for each of the geometry and material configurations described above. Two volumes have been scanned along the z direction: One volume with $7791\,\text{mm} < z < 8075\,\text{mm}$ containing the first SciFi station, and one volume with $7700\,\text{mm} < z < 7091\,\text{mm}$ containing the first IT station. The results of these scans are shown in Figure 5 for the radiation length fraction and interaction length fraction of a SciFi station, and in Figure 6 for the radiation length fraction and interaction length fraction of an IT station.

The scan of the radiation length for the IT station yields $X/X_0 = 1.4\%$ for the IT layer without DCDC, $X/X_0 = 2.5\%$ for the IT layer with DCDC and $X/X_0 = 7.0\%$ for the IT cables. These values are in good agreement with the input values derived in Sec. 3.2 above. The scan of the interaction length for the IT station yields $\lambda/\lambda_0 = 0.67\%$ for the IT layer without DCDC, $\lambda/\lambda_0 = 0.86\%$ for the IT layer with DCDC and $\lambda/\lambda_0 = 0.65\%$ for the IT cables.

The scans of radiation length and interaction length for the SciFi station yield $X/X_0 = 4.3\%$ and $\lambda/\lambda_0 = 2.4\%$ in areas with regular modules, outside of gaps and mirrors, while the areas where fibres have been removed have $X/X_0 = 2.7\%$ and $\lambda/\lambda_0 = 1.5\%$.

Finally, scans of the radiation length and interaction length fractions have been performed using a wider volume corresponding to a full downstream tracker station volume (containing one SciFi station and two IT stations) with $7700\,\text{mm} < z < 8165\,\text{mm}$. The results of these scans, shown in Figures 8 and 7 seem to indicate that the radiation length fraction is similar in the configurations 'Fibres cut (without DCDC)' and 'Module Cut (with DCDC)' while the interaction length fraction is lower for the latter option.

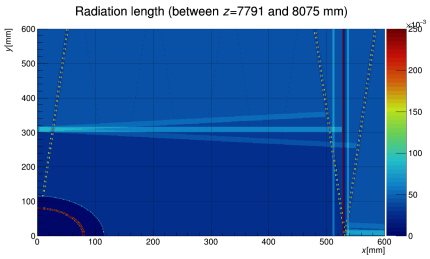

(a) X/X_0 : SciFi station, 'Fibres cut'

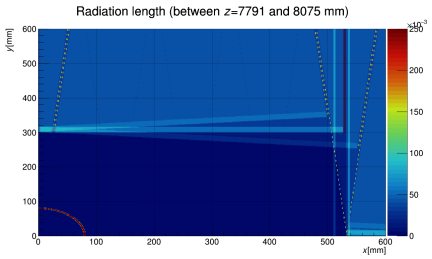

(b) X/X_0 : SciFi station, 'Module cut'

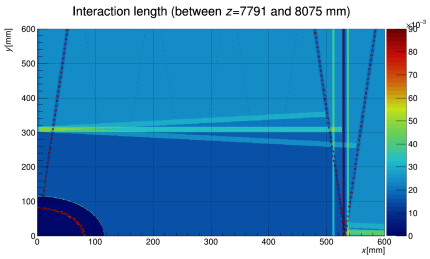

(c) λ/λ_0 : SciFi station, 'Fibres cut'

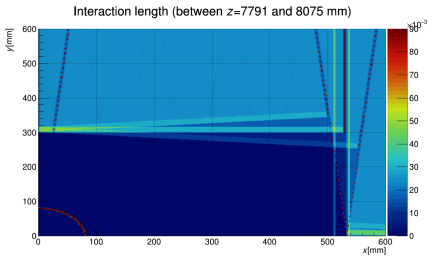

(d) λ/λ_0 : SciFi station, 'Module cut'

Figure 5: Scans of the radiation length fraction X/X_0 (plots a,b) and interaction length fraction λ/λ_0 (plots c,d) for one SciFi station in the geometry configurations: 'Fibres Cut' (a,c) and 'Module Cut' (b,d).

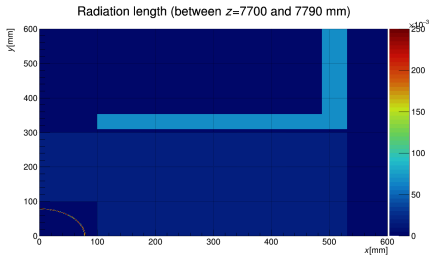

(a) X/X_0 : IT station, 'Without DCDC'

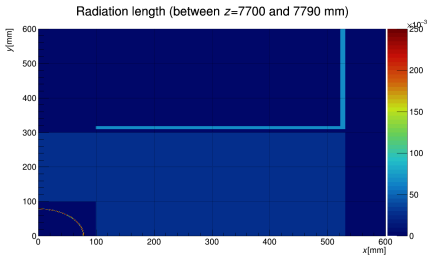

(b) X/X_0 : IT station, 'With DCDC'

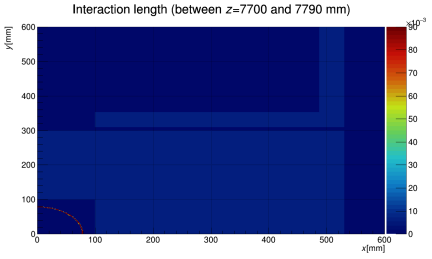

(c) λ/λ_0 : IT station, 'Without DCDC'

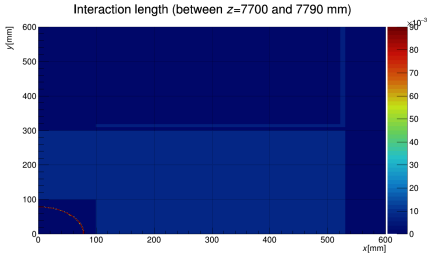

(d) λ/λ_0 : IT station, 'With DCDC'

Figure 6: Scans of the radiation length fraction X/X_0 (plots a,b) and interaction length fraction λ/λ_0 (plots c,d) for one IT station in the configurations: 'Without DCDC' (a,c) and 'With DCDC' (b,d).

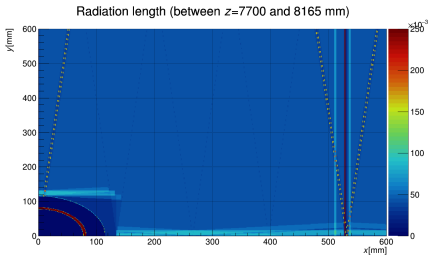

(a) X/X_0 : Downstream tracker station, 'Reference'

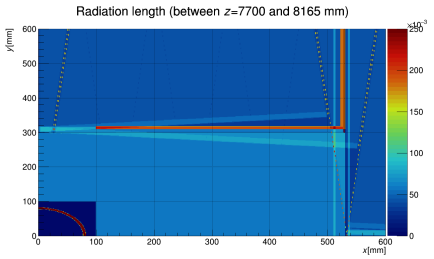

(b) X/X_0 : Downstream tracker station, 'Module Cut (with DCDC)'

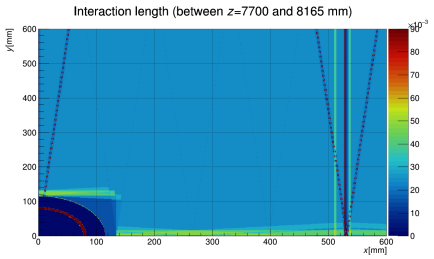

(c) λ/λ_0 : Downstream tracker station, 'Reference'

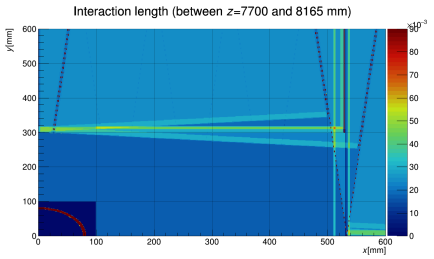

(d) λ/λ_0 : Downstream tracker station, 'Module Cut (with DCDC)

Figure 7: Scans of the radiation length fraction X/X_0 (plots a,b) and interaction length fraction λ/λ_0 (plots c,d) for one complete downstream tracker station (SciFi + IT) in the geometry configurations: 'Reference' (a,c) and 'Module Cut (with DCDC)' (b,d).

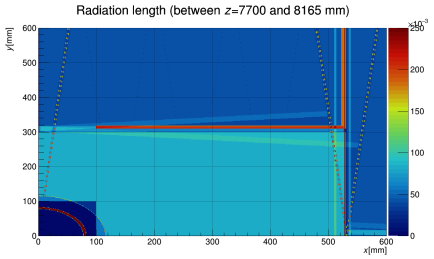

(a) X/X_0 : Downstream tracker station, 'Fibres Cut (with DCDC)'

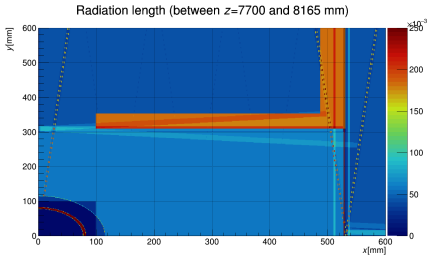

(b) X/X_0 : Downstream tracker station, 'Fibres Cut (without DCDC)'

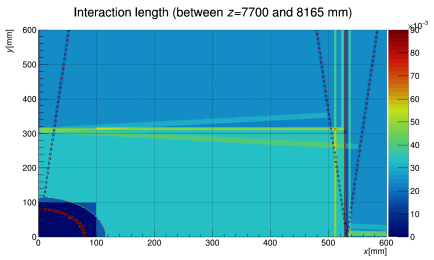

(c) λ/λ_0 : Downstream tracker station, 'Fibres Cut (with DCDC)'

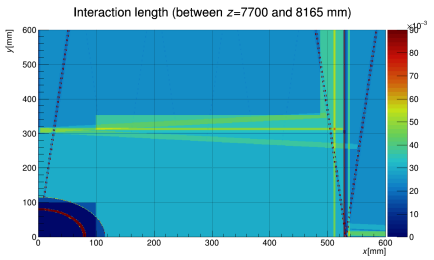

(d) λ/λ_0 : Downstream tracker station, 'Fibres Cut (without DCDC)'

Figure 8: Scans of the radiation length fraction X/X_0 (plots a,b) and interaction length fraction λ/λ_0 (plots c,d) for one complete downstream tracker station (SciFi + IT) in the geometry configurations: 'Fibres Cut (with DCDC)' (a,c) and 'Fibres Cut (without DCDC)' (b,d).

4 Data samples

The simulated data samples used in this study have been generated using GAUSS `v54r4`, which uses `LHCb v51r0`. The event generator is PYTHIA 8 and the interactions of particles with the material of the LHCb detector are handled by GEANT4 `v106r2p1`.

This study is based on datasets of fully simulated $B_s \to \phi\phi$ decay events, implementing different configurations of the Mighty Tracker geometry in LS3 enhancements as described in Section 3. The simulated beam conditions correspond to the Upgrade I conditions, with an instantaneous luminosity $\mathcal{L} = 2 \times 10^{33}\,\mathrm{cm}^{-2}\,\mathrm{s}^{-1}$. When recording real data, the LHCb magnet switches polarity so that approximately equal amounts of data are recorded with a magnetic field oriented upwards (Magnet Up) and downwards (Magnet Down). This allows to cancel out spatial asymmetries due to the presence of the magnetic field that can affect the measured observables. In order to gauge this effect, simulated datasets are generated for Magnet Up and Magnet Down polarities. The datasets are listed in Table 4 with the number of events generated for each of them.

Table 4: Numbers of $B_s \to \phi\phi$ decay events simulated for each magnet polarity and for each of the four geometry scenarios for the downstream tracker geometry. All simulations use Upgrade I beam conditions.

Scenario	Events (Magnet Up)	Events (Magnet Down)
Reference	917	921
Module Cut (with DCDC)	708	920
Fibres Cut (with DCDC)	690	913
Fibres Cut (without DCDC)	706	704

5 Definition of geometrical regions in the LHCb detector

In order to study the origins of secondary particles detected in the fibre layers and compare the contributions from various elements, the LHCb detector volume is broken down into regions corresponding to one or several subdetectors. The figures included in this section were obtained using event samples simulated for the Reference Geometry.

5.1 Definition of detector regions

The sub-detectors of the LHCb detector are oriented almost perpendicular to the z axis[1]. Therefore, a coarse definition of six detector regions, referred to as Regions I to VI, is made by applying one dimensional cuts along the z axis. The values of these cuts are listed in Table 5 and their positions are shown in Fig. 28 by the black lines overlaid on a plot of the (y, z) coordinates of the origins of secondary particles (as defined in Section 5.2) that generate hits in any of the SciFi layers. The equivalent distribution of origin coordinates

[1]The large sub-detectors downstream of the spectrometer magnet are mounted vertically (following gravity) while the z axis of the LHCb coordinate system follows the LHC beam axis. This leads to a small tilt of 3.601 mrad between these sub-detectors and the y axis of the LHCb coordinate system.

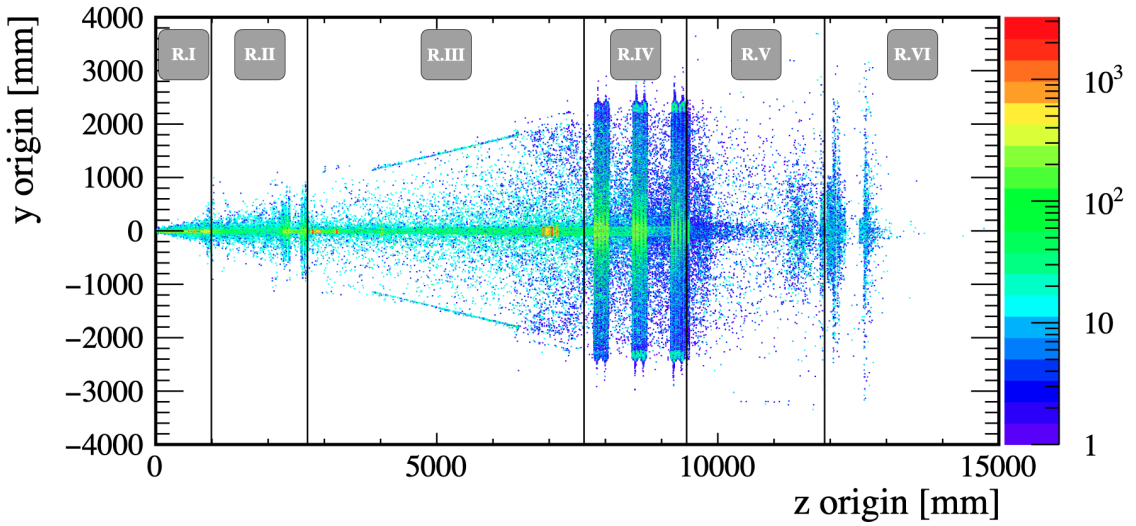

Figure 9: Scatter plot of the (z,y) coordinates of the origins of secondary particles generating hits in the SciFi for the Reference Geometry. Vertical black lines indicate the six detector regions (R.I-R.VI) defined for this study.

is also shown for the Module Cut Geometry in Appendix A. The LHC beampipe and different sub-detectors are clearly visible as sources of such secondaries. Region I contains the VELO, Region II includes RICH1 and UT, Region III covers the spectrometer magnet, Region IV contains the three downstream tracking stations, Region V includes RICH2, and Region VI any of the simulated material further downstream. The limit between Region IV and Region V is determined with particular care in order to separate cleanly the final SciFi layer and the RICH2 entrance window which are very close.

Table 5: Downstream limits for each of the six detector regions defined for this study. Region VI is unconstrained in the downstream direction, and Region I is unconstrained in the upstream direction.

Region	I	II	III	IV	V	VI
Downstream z limit (in mm)	990	2700	7620	9445	11900	$+\infty$

One of the most intense sources of secondaries producing hits in the SciFi is the structure of beampipe support collars and bellows at $z \approx 7000\,\text{mm}$, just upstream of the first downstream tracking station. The contribution from these aluminium bellows and support collars is included in Region III, together with the magnet, whose iron yoke is visible as two outward-going diagonal lines at positive and negative y. Some production of secondaries is also seen at zy positions outside of detector elements. This can be due to decays of long-lived particles and to interactions in air. No attempt is made here to distinguish between these two sources of secondaries. The downstream tracking stations themselves appear as a source of secondaries producing hits in the SciFi. In general, the production of secondaries is more intense closer to the beam axis, due to the higher flux of particles, underlining the importance of understanding the impact of the IT material on occupancies.

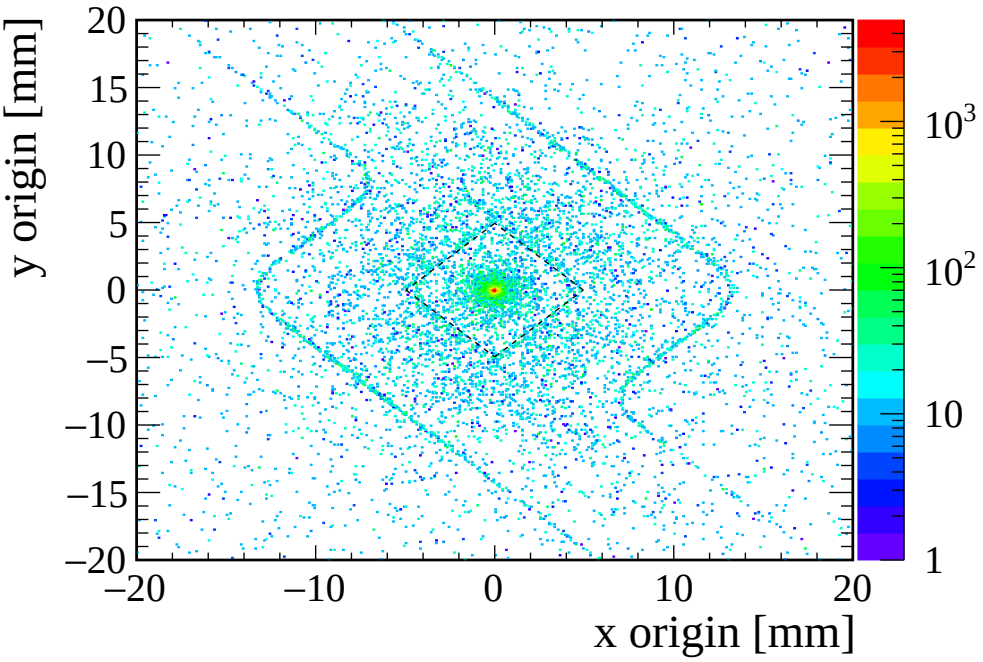

Figure 10: Distribution of the x, y positions of particle origins with $|z| < 500$. Some structure of the VELO modules is visible due to particles produced in interactions in their material. Particles with origin inside the region defined by the overlaid dashed black lines are assigned as "primary" particles; particles with origin outside this region are assigned as "secondary" particles.

5.2 Region I

Region I contains the *pp* interaction point and a large fraction of particles from Region I will be particles produced in the *pp* interaction or the decay products of such particles. In the following, we will refer to such particles as "primary". More than 90% of these particles can be identified by requiring that their origin be equal to their associated primary *pp* collision vertex[2]. Decay products of long-lived particles, however, will have an origin different from the *pp* collision vertex. Therefore, particles are also assigned here as "primary" if their origin falls inside a volume which stretches from $z = -500\,\text{mm}$ to $z = 500\,\text{mm}$ along the beam axis and is defined in the xy plane by a square of side length $2 \times 3.5\,\text{mm}$, rotated by 45° about the z axis. This shape avoids the material of the VELO detector, as illustrated in Fig. 10. Any particle which does not come from a primary vertex and does not come from the volume defined above will be considered a secondary particle. Note that any decay products of long-lived particles which travel sufficiently far to decay *outside* this volume will be incorrectly assigned as secondary particles.

5.3 Region IV

In order to identify the specific detector elements in which secondary particles are produced, Region IV has been separated into several approximated volumes associated to the different parts of the Mighty Tracker. The twelve SciFi layers of the three downstream tracking

[2]The simulation retains the position of the origin of each particle as well as the position of the *pp* interaction vertex to which the particle is associated.

stations are identified by cuts in the form of rectangles with central z position, dimensions and rotation angle specified in Tables 6 and 7. No distinction is made between secondaries produced within the fibres and those within the module housing of the SciFi layers. Separate volumes are also provided for the five Inner Tracker layers and attached cables in Table 7. The beampipe hole of dimensions 200 mm × 200 mm centred at $(x, y) = (0, 0)$ is excluded from all volumes. These prisms are given an additional contribution to their thickness of $\varepsilon = 0.5$ mm to provide some tolerance for origins situated at the edge of these materials.

Table 6: Position coordinates along the z axis for the centre of the volumes used to select origins in the stereo and x-layers of the SciFi, and in the layers of the IT.

Layer	Layer centre z coordinate (in mm)
IT layer 1	7754.0
SciFi X-layer 1	7826.3
SciFi St.1 U-layer	7896.1
SciFi St.1 V-layer	7965.9
SciFi X-layer 2	8035.7
IT layer 2	8108.0
IT layer 3	8436.0
SciFi X-layer 3	8508.3
SciFi St.2 U-layer	8578.1
SciFi St.2 V-layer	8647.9
SciFi X-layer 4	8717.7
IT layer 4	8790.0
IT layer 5	9121.0
SciFi X-layer 5	9193.3
SciFi St.3 U-layer	9263.1
SciFi St.3 V-layer	9332.9
SciFi X-layer 6	9402.7

5.4 Beampipe geometry

In Region IV, the geometry of the beampipe has been described by several conical volumes with the same parameters as defined in the detector database (DDDB) geometry description [11]. The origins of secondary particles generating hits in the SciFi which fall within these volumes are coloured blue in Figure 11. The beampipe in Region III & V is approximated by a cone that accounts for most of the material of the beampipe. This cone has a radius of 29.3 mm at the start of Region III and 120.7 mm at the end of Region V. The finer structure of the beampipe in Region III is complicated by the presence of the aluminium bellows and support collars. Six polycones are defined around the volumes containing these components. A polycone is a volume of revolution about the axis generated from the line connecting a series of (y, z) coordinates. The (y, z) coordinates of the implemented polycones are specified in Table 12 of the Appendix. Origins are coloured

Table 7: Centre position, dimensions and rotations for the cut volumes used to select origins in the twelve layers of the SciFi tracker and the five IT detectors (and cables). Cables (H) and cables (V) respectively refer to the horizontal and vertical parts of the cables as shown in Fig. 3 (a). The y' and z' coordinates indicate that the height and thickness are those dimensions oriented along the local y and z axes of the object after it has been rotated about the x axis. Full, not half, dimensions are provided. The dimensions used for the configuration without DCDC converters (and larger cables) in Fig. 3 (b) is shown between square brackets.

Volume	SciFi layer	IT layer	Cables (H)	Cables (V)
x position of the centre (in mm)	0.0	0.0	315	525.75 [508.75]
y position of the centre (in mm)	0.0	0.0	314.25 [331.25]	1706.75
rotation about $\hat{x}$ (in rad)	-3.601	-3.601	-3.601	-3.601
width along x (in mm)	$+\infty$	1060	430	8.5 [42.5]
height along y' (in mm)	$+\infty$	600	8.5 [42.5]	2776.5
thickness along z' (in mm)	$41.57 + \varepsilon$	$29.9[29.3] + \varepsilon$	1.0	1.0

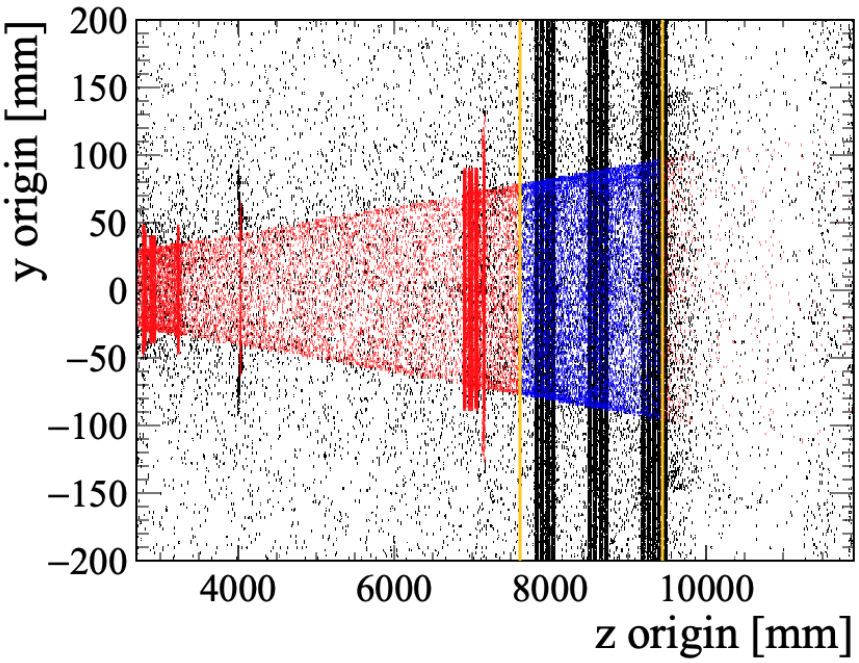

Figure 11: Position (y, z) of the origins of secondary particles in Regions III, IV and V. The beampipe in Region IV is defined by conical volumes reproducing the same volumes specified in the DDDB geometry description. The origins within these volumes are shown in blue. In Region III and V the beampipe is defined by a cone with opening angle $\sim 10\,\text{mrad}$, as well as six polycones for the bellows and collars in Region III with the parameters specified in Table 12 of the Appendix. The origins within these volumes are shown in red. The orange vertical lines show the limits of Region IV.

red in Figure 11 where they fall within this description in Region III & V. The stainless steel support cables are not included in this description, as can be seen in Figure 11 by the clustered origins in black at $z \sim 4\,\text{m}$.

6 Hits from secondary particles in the SciFi region

The occupancy studied in this note is defined in the next section based on hits, *i.e.* interactions of particles with the material of the detector. In this section, these interactions will be characterised via the distributions of the deposited energy, time since proton-proton interaction, and momentum of the particles incident on the SciFi.

As in the previous sections, the geometry description of the active area covered by the SciFi is modified to exclude the area covered by the IT. The configuration studied here corresponds to the Reference geometry (with Magnet Up orientation).

Figure 12 shows the energy deposited by incoming particles in the SciFi in Layer 1 and Layer 6. It is seen that particles from secondary interactions tend to deposit more energy than those from primary interactions, owing to their lower momentum (as will be shown in Figure 13). Also, the total amount of energy deposited in Layer 6 is higher than in Layer 1, which is further upstream. In each of these layers, the contributions of the hits have been broken down following the origins of the incoming particles. In Layer 1, 25 % of the total amount of energy deposited comes from the SciFi and 28 % from the beampipe, while in Layer 6 these fractions are 43 % and 17 % respectively. Layer 6 is sensitive to secondaries produced in the upstream SciFi layers, but is less sensitive to the beampipe which is screened by the upstream detector material. The amount of energy deposited by particles originating in the same layer is however very similar in Layers 1 and 6.

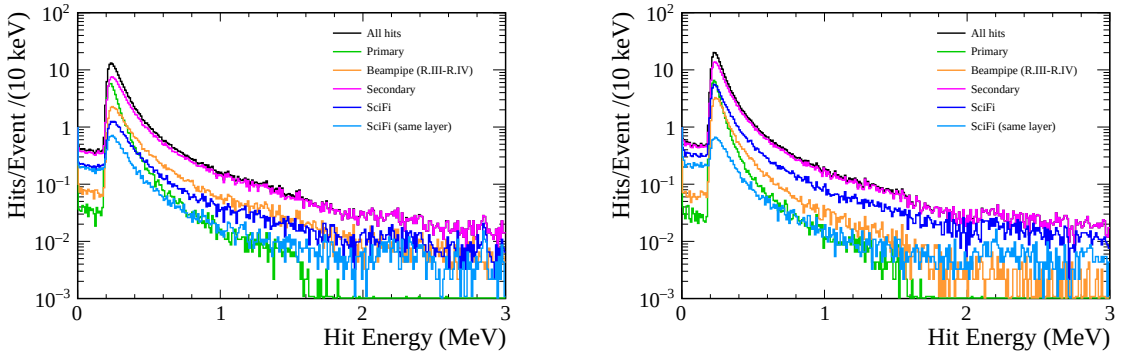

(a) Layer 1 (b) Layer 6

Figure 12: Energy deposited in the fibres by particles interacting with Layer 1 (left) and Layer 6 (right).

More information about the hits recorded in the SciFi Tracker is given by the distribution of momenta of the incoming particles shown in Fig. 13. Particles from primary interactions which interact in the SciFi tracker typically have momenta above 800 MeV/c, while particles from secondary interactions in the SciFi tend to have a much lower momentum. The fraction of particles with very low momentum, below 10 MeV/c, is $(5.16 \pm 0.05)\%$ in Layer 1, and $(8.72 \pm 0.06)\%$ in Layer 6. For more detail, distributions of the fraction of incoming particles with momenta below fixed thresholds are shown in Fig. 31, in appendix C for all the SciFi x-layers.

The time duration between the primary interaction (proton-proton collision) responsible for production of a given particle and its subsequent interaction with a SciFi layer can be seen in Fig. 14 for the hits in SciFi layers 1 (left) and 6 (right). Note that for secondary

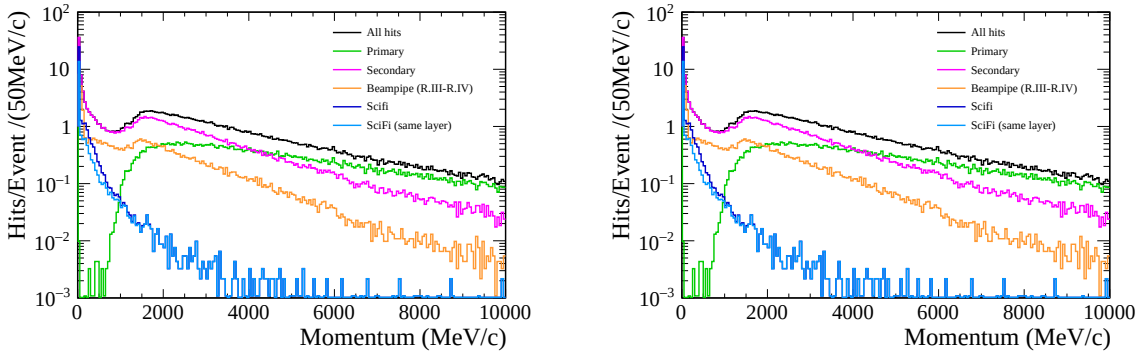

(a) Layer 1 (b) Layer 6

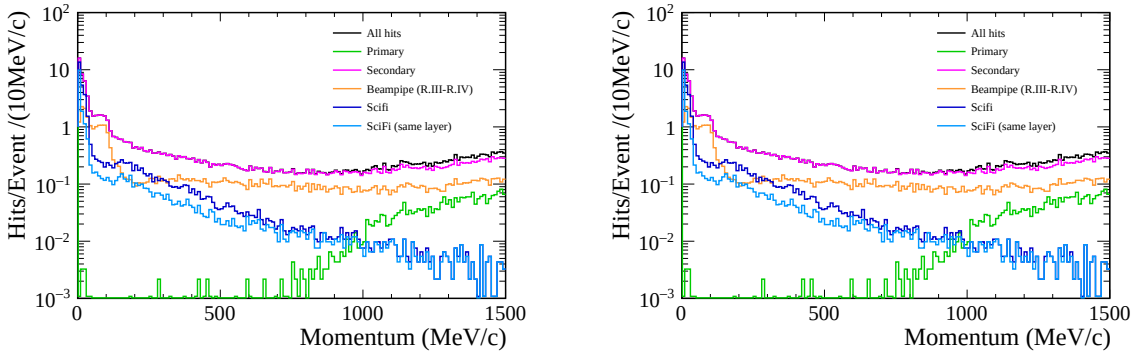

(c) Layer 1 (d) Layer 6

Figure 13: Momentum distributions of incoming particles with hits in Layer 1 (upper left) and Layer 6 (upper right) of the SciFi. A zoom on the low momentum region is shown for Layer 1 (lower left) and Layer 6 (lower right).

particles, the time of the primary interaction (where the first ancestor of the secondary particle is created in the proton-proton collision) is different from the time of the secondary interaction (when the secondary particle itself is created). For Layer 1, it can be seen that a propagation time of 26 ns is needed for the fastest particles to travel between the proton-proton collision point and the sensitive material. After this delay, all the particles from the primary interaction are seen within 15 ns. Secondary particles however can have much longer propagation times. In particular, a secondary peak can be seen at 60 ns in Layer 1 and at 55 ns in Layer 6. These hits correspond mainly to secondary particles that are produced downstream of the considered layer but back-scatter in the upstream direction. This is clarified in Fig. 14, where the contribution from secondary particles to the total number of hits is divided between those moving in the downstream direction (forwards) and those moving in the upstream direction (backwards). In Layer 1, 88 % of the hits with a propagation time between 54 and 66 ns are from particles travelling backwards. In Layer 6, backwards hits make up 87 % of the hits with a propagation time between 49 and 62 ns. Out of the backwards hits in this time window in Layer 6, 46 % come from Region V, and 31 % from Region VI. The coordinates of the origins of hits seen in the secondary peak in Layers 1 and 6 are shown in appendix D, in Fig. 32.

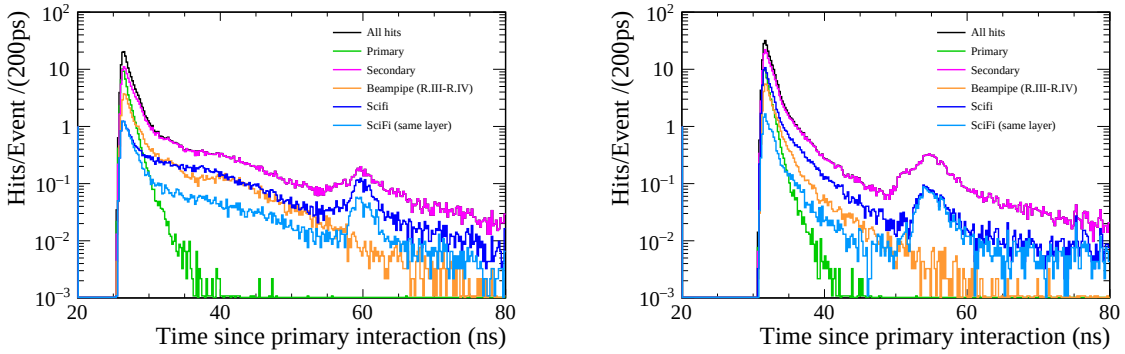

(a) Layer 1

(b) Layer 6

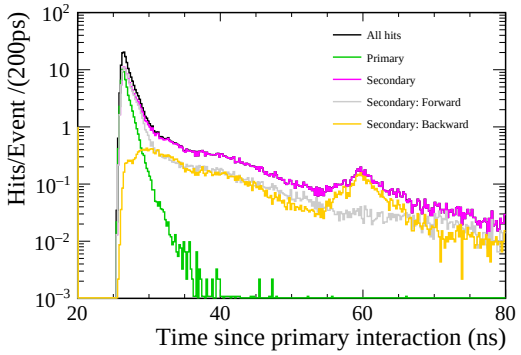

(c) Layer 1

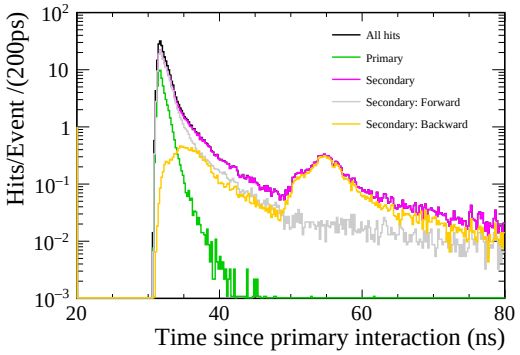

(d) Layer 6

Figure 14: Distributions of the time since the primary interaction for hits in SciFi Layer 1 (left) and Layer 6 (right). A breakdown in terms of regions of origins is given in the top row. In the bottom row, the contributions of hits from secondary interactions are separated between those coming from particles travelling backwards and forwards.

7 Occupancy Determination

In this section, the definition of the occupancy as it is used throughout this study will be given, and the difference between this definition and the channel occupancy (percentage of SiPM channels activated) will be underlined and explained.

7.1 Definition of occupancy

The occupancy in the SciFi is defined here as the fraction of fibres hit by at least one particle in any given event. As noted in Section 2, a fibre is defined here by a 250 μm wide interval in the x direction, extending in the vertical direction from the centre of the SciFi Tracker until the outer edge of the acceptance at the top or the bottom of the detector. Particle densities are assumed to be symmetric about $y = 0$ and occupancies are averaged over the upper and lower halves of the detector. Plots and numbers are shown assuming a constant cluster size of 1, i.e. a particle crossing the active area of a SciFi layer activates exactly one fibre.

Average occupancies as a function of x are determined by counting the number $F_i(x)$ of fibres hit in event i within a group of B contiguous fibres centred around x and taking

the average over all simulated events:

$$\mathcal{O}_{avg}(x) = \frac{1}{N_{\text{evts}}} \cdot \sum_{i}^{N_{\text{evts}}} \frac{F_i(x)}{2B} = \frac{1}{N_{\text{evts}}} \cdot \sum_{i}^{N_{\text{evts}}} \mathcal{O}_i(x)\,, \tag{1}$$

where the factor $2B$ in the denominator is due to the averaging over the top and bottom halves of the detector. An example of such a distribution is shown in Figure 15(a). A group size of $B = 80$ is used here and throughout this study. Figure 15(b) shows an example of the event-by-event fluctuation in $O_i(x)$, for a group of $B = 80$ fibres centred around $x = 550$ mm.

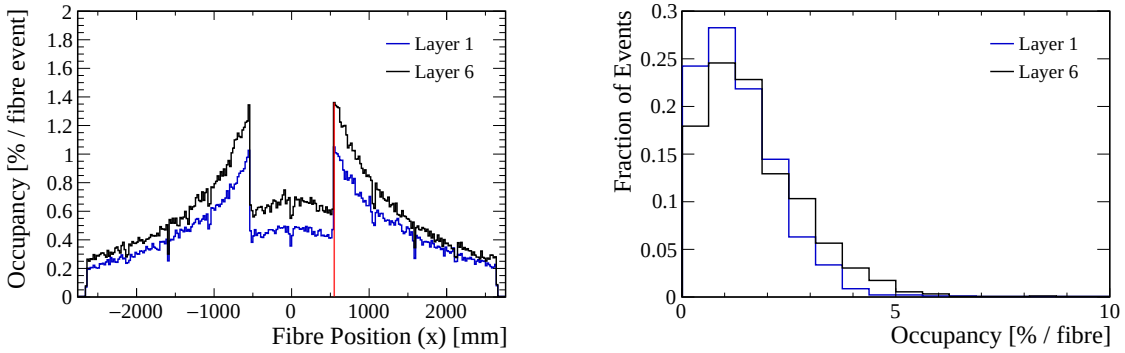

(a) Average Occupancy, B=80

(b) Occupancy (by event), $540\,\text{mm} < x < 560\,\text{mm}$

Figure 15: The average occupancy in Layers 1 and 6 of the Reference geometry is shown in (a) as a function of the fibre position along the x axis. The bin, of width $B = 80$ fibres, centred at 550 mm is highlighted in red, indicating the fibre group chosen to evaluate the occupancy by event, as shown in (b). The choice of a bin size in (b) of $1/2B = 0.625\%$/fibre in occupancy is explained in Sec. 9.5. Events are simulated with Magnet Up.

As noted in Table 4, event samples for each simulation scenario have been simulated for both magnet polarities ('Magnet Up' and 'Magnet Down'). The occupancy is distributed differently over x for the two magnet polarities due to the charge asymmetry of the particle production (two protons are present in the initial state before collision, leading to a left/right asymmetry in the distribution of charged particles downstream of the magnet). Figure 16 shows this effect, with the occupancy slightly higher at $x > 0$ for the 'Magnet Up' orientation, and vice versa. The average occupancies in the fibre group at $x = +550$ mm is $1.050 \pm 0.027\%$ ($1.361 \pm 0.030\%$) in Layer 1 (Layer 6) for 'Magnet Up' while it is $0.991 \pm 0.026\%$ ($1.292 \pm 0.030\%$) in Layer 1 (Layer 6) for 'Magnet Down'.

7.2 Estimating the effect of cluster size

In the absence of a simulation of the detector response, the results shown in this study assume a constant cluster size of one, i.e. a particle crossing the active area of the SciFi is assumed to activate exactly one fibre and one readout channel. In reality, it is expected [12] that the most probable cluster size in the SciFi is 2 and that the average cluster size is approximately 2.6.

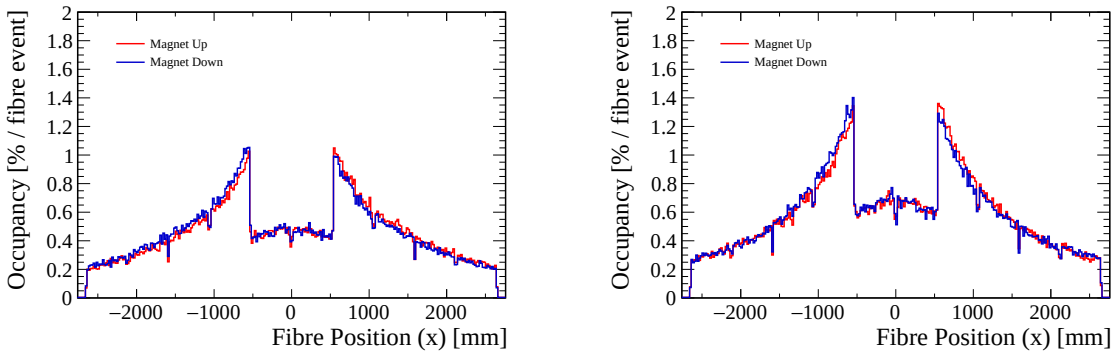

(a) Layer 1 (b) Layer 6

Figure 16: Occupancy for the Reference Geometry as a function of the fibre position for simulated data samples generated with the Magnet Up (red line) and Magnet Down (blue line) configurations. Groups of 80 fibres are used.

Estimates of the true expected occupancies in the SciFi can be obtained to first order by simply multiplying all values shown in this note by the expected cluster size. This simple scaling will lead to a slight overestimation of the true occupancy, since fibres that belong to two overlapping clusters will be counted twice. A simple toy study has been performed here to quantify the possible size of this overestimation:

1. The occupancy $O(n_C)$ for a fixed cluster size n_C was estimated by activating for each hit the n_C fibres closest to the x position of the hit and then calculating the occupancy as defined in Section 7.1 above, counting each activated fibre once.

2. The occupancies obtained assuming cluster size one were scaled by the assumed fixed cluster size n_C, i.e. $n_C \times O(1)$.

3. The ratio $R = n_C \times O(1) \,/\, O(n_C)$ of the two results was calculated and a one-sided upper 90% confidence interval on R was determined.

The comparison was performed for $n_C = 2, 3, 4$ and for the combined 'Magnet Up' and 'Magnet Down' samples in the Reference geometry. Results for the groups of peak fibres centred around $|x| = \pm 550$ mm are shown in Table 8. Results for the groups of central fibres at $|x| < 540$ mm are shown in Table 9.

Table 8: Comparison of occupancy estimations for cluster size n_C in the groups of peak fibres. See the main text for explanations of the variables. The digits given in parentheses indicate the statistical uncertainty on the last digit of the corresponding value.

Layer	1	2	3	4	5	6
Cluster size: $n_C = 2$						
$O(n_C)$ [%/fibre.event]	2.05(3)	2.35(3)	2.27(3)	2.55(3)	2.29(3)	2.68(3)
$n_C \times O(1)$ [%/fibre.event]	2.06(4)	2.37(4)	2.28(4)	2.57(4)	2.30(4)	2.70(4)
$R = n_C \times O(1) \,/\, O(n_C)$	1.00(2)	1.01(2)	1.01(2)	1.01(2)	1.01(2)	1.01(2)
90% C.L. (R)	1.032	1.036	1.033	1.034	1.034	1.031
Cluster size: $n_C = 3$						
$O(n_C)$ [%/fibre.event]	3.05(3)	3.48(3)	3.37(3)	3.77(4)	3.39(3)	3.97(4)
$n_C \times O(1)$ [%/fibre.event]	3.09(6)	3.55(6)	3.42(6)	3.85(6)	3.45(6)	4.05(6)
$R = n_C \times O(1) \,/\, O(n_C)$	1.01(2)	1.02(2)	1.02(2)	1.02(2)	1.02(2)	1.02(2)
90% C.L. (R)	1.041	1.046	1.041	1.047	1.044	1.043
90% C.L. (R)	1.041	1.046	1.041	1.047	1.044	1.043
Cluster size: $n_C = 4$						
$O(n_C)$ [%/fibre.event]	4.04(4)	4.12(8)	4.46(4)	4.99(4)	4.49(4)	5.53(4)
$n_C \times O(1)$ [%/fibre.event]	4.12(8)	4.74(8)	4.56(8)	5.14(8)	4.60(8)	5.40(9)
$R = n_C \times O(1) \,/\, O(n_C)$	1.02(2)	1.03(2)	1.02(2)	1.03(2)	1.03(2)	1.03(2)
90% C.L. (R)	1.047	1.054	1.048	1.054	1.050	1.050

Table 9: Comparison of occupancy estimations for cluster size n_C in the central fibres. See the main text for explanations of the variables. The digits given in parentheses indicate the statistical uncertainty on the last digit of the corresponding value.

Layer	1	2	3	4	5	6
Cluster Size: $n_C = 2$						
$O(n_C)$ [%/fibre.event]	0.910(2)	1.057(3)	1.06(3)	1.171(3)	1.107(3)	1.277(3)
$n_C \times O(1)$ [%/fibre.event]	0.912(4)	1.060(4)	1.008(4)	1.177(4)	1.110(4)	1.284(5)
$R = n_C \times O(1) \,/\, O(n_C)$	1.002(5)	1.003(5)	1.002(5)	1.005(4)	1.003(4)	1.006(4)
90% C.L. (R)	1.0077	1.0091	1.0080	1.0103	1.0082	1.0109
Cluster Size: $n_C = 3$						
$O(n_C)$ [%/fibre.event]	1.354(3)	1.571(3)	1.495(3)	1.739(3)	1.646(3)	1.893(4)
$n_C \times O(1)$ [%/fibre.event]	1.367(5)	1.590(6)	1.512(6)	1.765(6)	1.665(6)	1.926(7)
$R = n_C \times O(1) \,/\, O(n_C)$	1.010(5)	1.012(4)	1.011(4)	1.015(4)	1.012(4)	1.017(4)
90% C.L. (R)	1.0153	1.0178	1.0165	1.0205	1.0170	1.0225
Cluster Size: $n_C = 4$						
$O(n_C)$ [%/fibre.event]	1.803(3)	2.088(4)	1.990(4)	2.308(4)	2.189(4)	2.513(4)
$n_C \times O(1)$ [%/fibre.event]	1.823(7)	2.121(8)	2.015(8)	2.353(9)	2.220(8)	2.568(9)
$R = n_C \times O(1) \,/\, O(n_C)$	1.011(4)	1.016(4)	1.013(4)	1.013(4)	1.020(4)	1.014(4)
90% C.L. (R)	1.0170	1.0211	1.0185	1.0248	1.0195	1.0268

8 Origins of the secondary particles in the Mighty Tracker

The main concern with secondary particles in the downstream tracker region is that they might increase the occupancy in the SciFi Tracker beyond acceptable levels. In this section, the various sources contributing to the occupancy in the Mighty Tracker will be identified by studying the origins of secondary particles that hit the scintillating fibres. The fraction of occupancy coming from each region of the detector will be quantified and the effect of secondary particle production within the stations and layers of the SciFi tracker itself will be considered in detail.

8.1 Origin-distinguished occupancy in the Mighty Tracker

In this section, the Reference Geometry is considered so as to provide a baseline before studying the effects of introducing additional material into the detector geometry description. Although the IT is not present and the fibres extend to the beampipe (equivalent to Upgrade I detector), only those hits which enter the fibre in the xy zone that would be outside the IT (with $|x| > 530\,\text{mm}$ and $|y| > 300\,\text{mm}$) are included in the occupancy. This allows for consistent comparison to the later simulations where the fibres only cover this region outside the IT.

An important element of the origin-distinguished occupancies determined in this work is the procedure that allows the assignment of an origin to the activated fibres with multiple hits in the same event. In these instances, one of the hits is chosen randomly and the origin of this particular hit is assigned to that 'activated fibre' which actually had multiple hits (possibly with very different origins). In assigning the origin of a contribution to the occupancy, only the position at which the particle which caused the hit in the fibre was created is considered. The origin assigned to an occupancy contribution is always that of the particle responsible for the hit. If the particle is generated in the detector material from a secondary particle, the source of this parent is not considered.

Figure 17 provides a breakdown of the occupancy according to the regions of the detector defined by their extent along the axial (z) direction. In the first layer of the SciFi tracker, shown in Figure 17 (a), the largest contribution arises from Region III which contains the magnet. The dominant source of secondary particles in this region is the beampipe, especially the support collars and bellows made of aluminium and stainless steel that are situated in this region.

This can be seen in Table 10, where the relative contribution of the beampipe from Regions III, IV and V is estimated with respect to the contribution from the same regions, and with respect to the total occupancy. In Layer 1 for example, the beampipe in Region III accounts for a fraction of $(82.26 \pm 0.22)\,\%$ of the occupancy from Region III, making it the leading source of secondary particles in this region. The contribution from the beampipe in Region III is even significant with respect to the total occupancy as it accounts for a fraction of $(26.503 \pm 0.070)\,\%$ of the total occupancy in Layer 1. However, the beampipe in Region IV has a much lower effect on the occupancy in Layer 1. It only contributes $(9.422 \pm 0.099)\,\%$ of the occupancy from Region IV, and $(1.653 \pm 0.017)\,\%$ of the total occupancy in this layer. Even in Layer 6, where this latter contribution is expected to be maximal (since Layer 6 is located near the downstream edge of Region

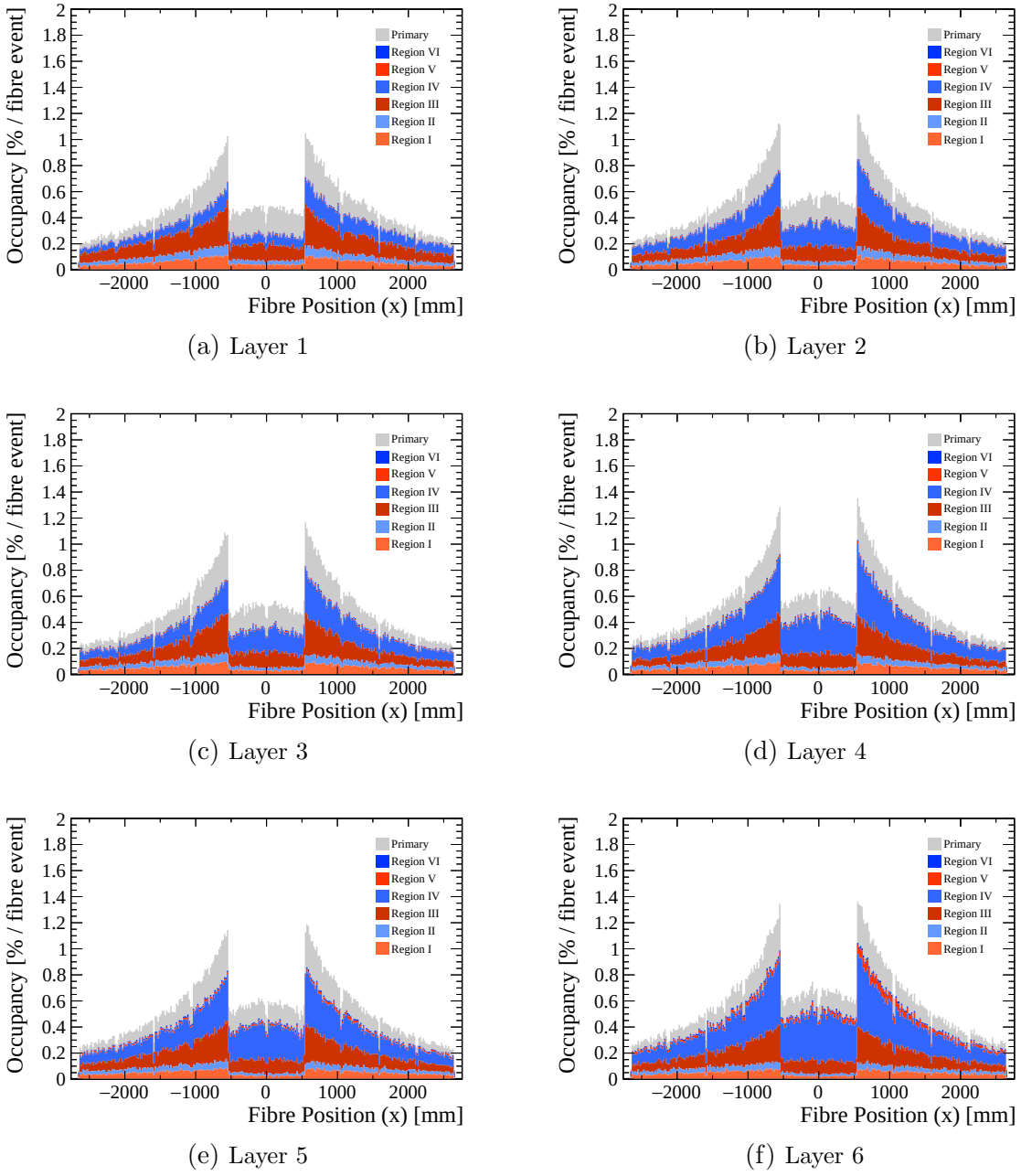

(a) Layer 1 (b) Layer 2

(c) Layer 3 (d) Layer 4

(e) Layer 5 (f) Layer 6

Figure 17: Occupancy for the Reference Geometry as a function of the fibre position, where the contributions from primary particles and secondary particles from different regions of the detector are distinguished in various colours. Bins of 80 fibres are chosen and events are simulated with Magnet Up.

IV), the beampipe in Region IV accounts only for $(6.482 \pm 0.047)\,\%$ of the occupancy from Region IV, and $(2.636 \pm 0.019)\,\%$ of the total occupancy.

Figure 18 illustrates once again the high occupancies from the beampipe in Region III with respect to the beampipe in other regions IV and V. The same figure also shows that the occupancy distribution from secondary particles from the beampipe are more peaked than the distributions of other detector elements as seen in Figure 17, due to the

fact that the material of the beampipe is more concentrated towards the centre than that of the SciFi or the IT.

Table 10: Contributions of the secondary particles coming from the beampipe in Regions III, IV and V for each SciFi x-layer. The contributions are averaged over all fibres in each layer and for events with both up and down polarities of the magnet. For each SciFi x-layer, the contribution from the beampipe in a given region is expressed as a fraction of the occupancy from the same region and as fraction of the total occupancy. The rightmost column shows the mean relative contribution over all layers. The digits given in parentheses indicate the statistical uncertainty on the last digit of the corresponding value.

SciFi layer	1	2	3	4	5	6	Mean over layers
R.III beampipe over R.III contribution	0.823(2)	0.828(2)	0.839(2)	0.843(2)	0.844(2)	0.847(3)	0.836(1)
R.III beampipe over total occupancy	0.2650(7)	0.2188(6)	0.2202(6)	0.1879(5)	0.1939(6)	0.1673(5)	0.2066(2)
R.IV beampipe over R.IV contribution	0.094(1)	0.0717(7)	0.0803(7)	0.0644(5)	0.0810(6)	0.0648(5)	0.0732(3)
R.IV beampipe over total occupancy	0.0165(2)	0.0204(2)	0.0221(2)	0.0239(2)	0.0276(2)	0.0264(2)	0.02306(8)
R.V beampipe over R.V contribution	0.054(4)	0.052(4)	0.050(3)	0.054(3)	0.054(2)	0.060(2)	0.056(1)
R.V beampipe over total occupancy	0.00032(2)	0.00035(2)	0.00047(3)	0.00059(3)	0.00104(4)	0.00233(6)	0.00091(2)

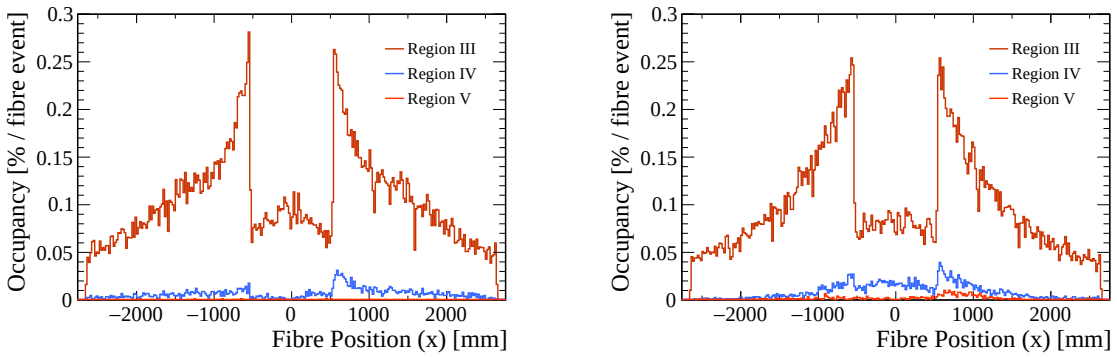

(a) Layer 1 (b) Layer 6

Figure 18: Occupancies from secondary particles coming from the beampipe in Regions III (dark red line), IV (blue line) and V (red line) for the Reference Geometry, shown as a function of the fibre position. Groups of 80 fibres are used and events are simulated with Magnet Up.

Plots (a)-(f) of Figure 17 demonstrate that the occupancy increases towards the downstream layers. Region IV is the dominant source of this trend, since the upstream layers progressively enter the acceptance of those downstream.

Figure 19 (a) and (b) show the same occupancy as a function of fibre position for Layer 1 and Layer 6, but the stacked histogram is instead constructed according to the different types of sources for secondary particles. All regions besides Region IV are considered 'Other', as well as anything not explicitly defined for the Region IV geometry breakdown (e.g. air, beampipe), since these parts of the geometry will be unchanged across the

different simulations considered in this work. The contributions of secondary particles are assigned to each type by identifying the origins inside the volumes defined in Section 5.3. Secondaries from the tracking stations are shown in blue, and the same increasing trend towards the downstream layers is evident as for Region IV in Figure 17. The volume in which the detector material of the IT has been added in later simulations is also distinguished (and similarly the volumes for the horizontal and vertical cables). There is a very small contribution from these volumes due to the air that occupies these volumes in this simulation for the Reference Geometry. An alternative method of presenting

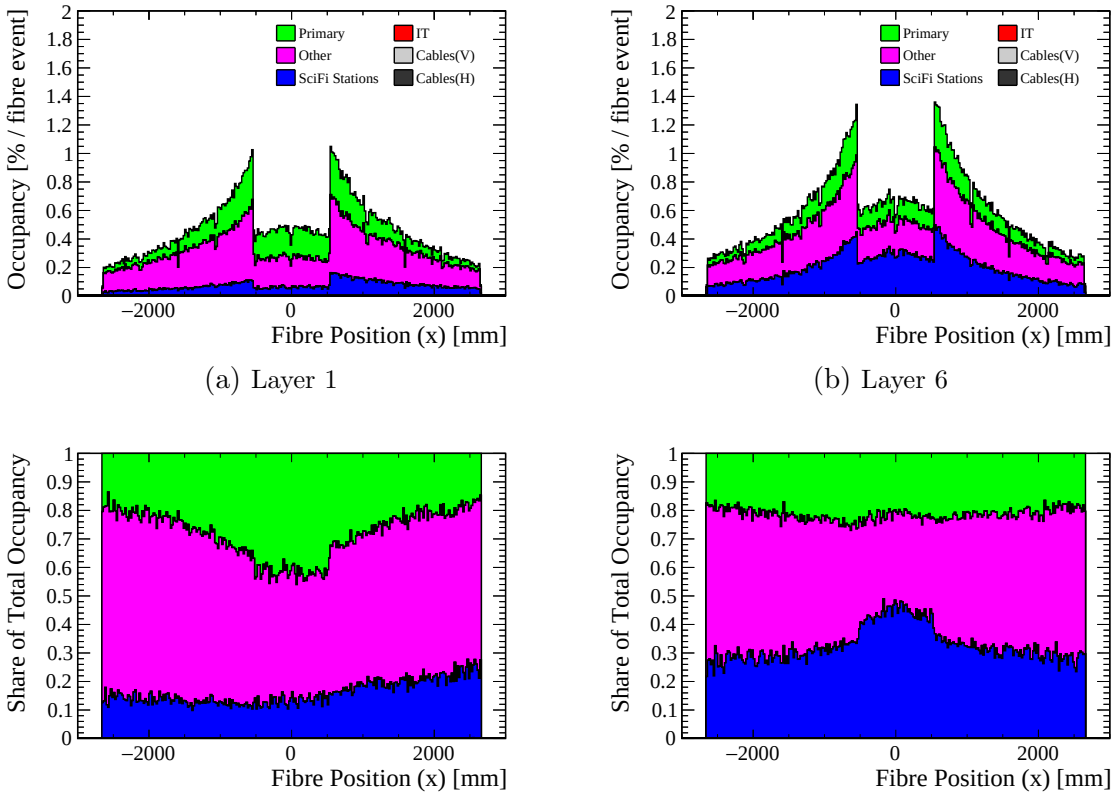

(a) Layer 1 (b) Layer 6

(c) Layer 1 (d) Layer 6

Figure 19: Occupancy and share of the total occupancy for Layers 1 and 6 as a function of the fibre position for the Reference Geometry, with the stacked contributions from primary particles (in green) and secondary particles from IT layers (in red, not visible for the reference geometry), horizontal and vertical cables (in grey, not visible either), SciFi stations (in blue) and other sources (in magenta). A bin size of 80 fibres is used and events are simulated with Magnet Up.

the stacked histograms for fibre occupancy is provided in Figure 19 (c) and (d). The vertical axis represents the share of the total occupancy at the given fibre position. This is determined by taking the occupancy histograms from (a) and (b) and dividing each of the stacked components by the value of the total occupancy at each group position. This representation allows for easier interpretation of the *relative* contributions of different sources of secondary particles and how they vary over the transverse extent of the tracker. The contribution of the stations increases downstream, from $10 - 20\%$ share of total occupancy in Layer 1 to $30 - 45\%$ share in Layer 6. In the central fibre groups, a bump appears towards the downstream layers which is due to secondaries from the stations.

This central region corresponds to hits in the fibres above and below the zone excluded by the IT. Since the downstream tracking layers measure secondaries produced in their upstream counterparts, and secondaries form abundantly due to the high incident particle flux close to the beampipe, the fibres closest to the beampipe experience a larger increase in occupancy due to this effect. This explains the bump in the share of total occupancy around $x = 0$.

A detailed breakdown of the contributions to the occupancy only from Region IV is presented in Figure 20. The three downstream tracking stations are each coloured in four shades of violet, blue and cyan respectively. In the upstream layer of each station, the dominant source of secondaries from within Region IV is the layer itself. This is true for the downstream layer of each station as well, but these layers experience a similar contribution from the upstream x-layer and the u, v-layers of the same station. The small contribution of downstream layers in the same station to the occupancy in the upstream x-layer, and the yet smaller contribution of layers in downstream stations (e.g. the small cyan stack for Station 3 visible in the Layer 1 and Layer 2 plots) indicates that backscattering of secondaries does not contribute significantly to the occupancy. Looking across all of the layers, the jump in occupancy between the first and last layer of a given station is mainly driven by secondaries from this same station. This jump is visible in violet in Figures 20 (a) and (b) for occupancies from Station 1 in Station 1, in blue in Figures 20 (c) and (d) for occupancies from Station 2 in Station 2, and finally in cyan in Figures 20 (e) and (f) for occupancies from Station 3 in Station 3. Overall, the effect dominating the increase in occupancy over the six layers is the additional material in the acceptance of the respective layer, with the highest occupancies reached at the most downstream position, in Layer 6.

9 Comparison of Mighty Tracker design options in terms of occupancy

In this section, the possibility of distinguishing several sources of secondary particles is used to study in detail the effect of modifying the SciFi stations and of adding DCDC converters to the IT layer material. The event-by-event fluctuations of the occupancy are also studied to inform potential cuts on occupancy to be used in reconstruction or data transmission software. Finally, the four configurations of the downstream tracker considered in this work are compared in terms of occupancy in the x-layers of the SciFi tracker.

9.1 Origin-distinguished occupancy for upgraded geometry scenarios

The occupancy in the fibres of SciFi x-layers can also be broken down between different sources for the three geometry scenarios including IT stations. Figure 21 shows the same distributions as Fig. 19, but for the 'Module Cut (with DCDC)' configuration instead of the Reference Geometry. Here, the contribution from the IT to the occupancy is clearly visible and amounts to $\sim 10\%$ of the occupancy in the peak fibre groups. The contribution from the cables also starts to appear in Fig. 21(d). Similar distributions have

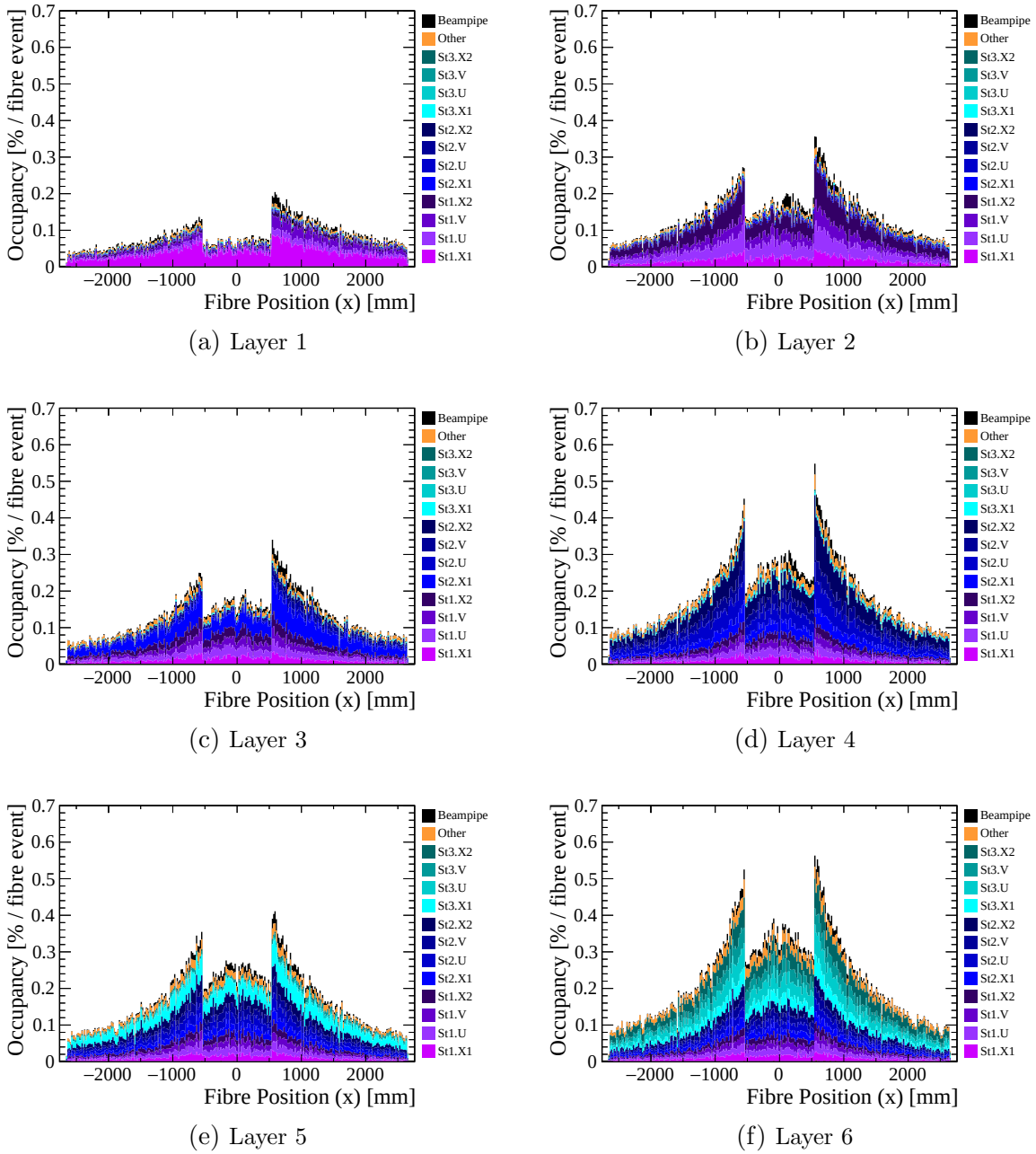

(a) Layer 1 (b) Layer 2

(c) Layer 3 (d) Layer 4

(e) Layer 5 (f) Layer 6

Figure 20: Occupancy contribution from secondaries produced in Region IV, for the Reference Geometry. The contribution from Region IV in Figure 17 is extracted and broken down according to the various sources of secondaries in this region. Note the lower vertical scale compared to earlier figures. The occupancy is plotted over fibre position in groups of 80 fibres, for events simulated with Magnet Up.

also been obtained for the 'Fibres Cut (with DCDC)' and 'Fibres Cut (without DCDC)' configurations and are shown in Fig.29 and 30 of the Appendix, respectively.

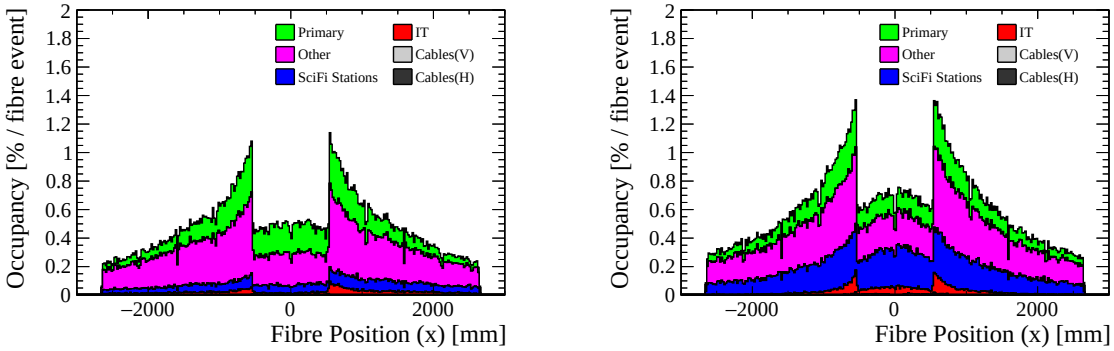

(a) Layer 1

(b) Layer 6

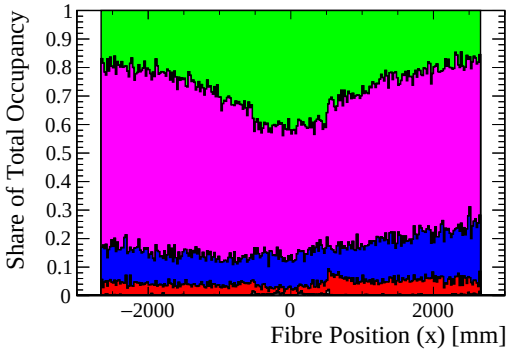

(c) Layer 1

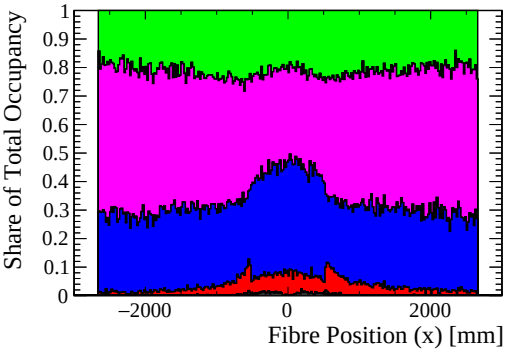

(d) Layer 6

Figure 21: Occupancy and share of the total occupancy for Layers 1 and 6 as a function of the fibre position for the geometry 'Module Cut (with DCDC)', with the stacked contributions from primary particles (in green) and secondary particles from IT layers (in red), horizontal cables (dark grey), vertical cables (light grey), SciFi stations (in blue) and other sources (in magenta). A bin size of 80 fibres is used and events are simulated with Magnet Up.

9.2 Comparison of SciFi Tracker Modifications

There are two possible alternatives considered in this work for the modification of the SciFi Tracker: 'Module Cut' and 'Fibre Cut', as defined in Section 3.1 and shown in Figure 4.

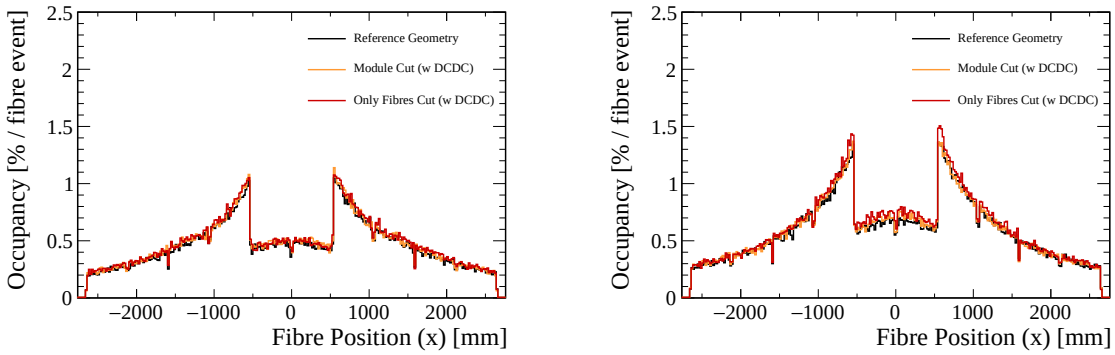

(a) Total, Layer 1

(b) Total, Layer 6

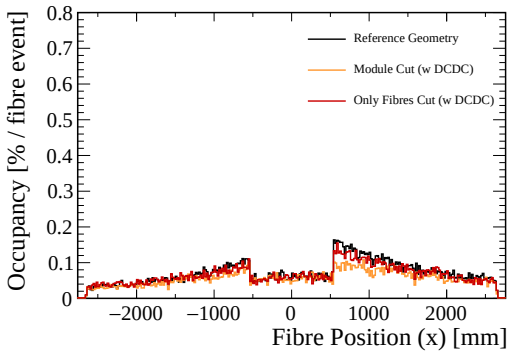

(c) SciFi Stations, Layer 1

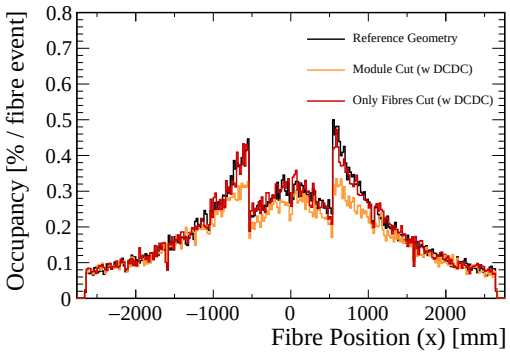

(d) SciFi Stations, Layer 6

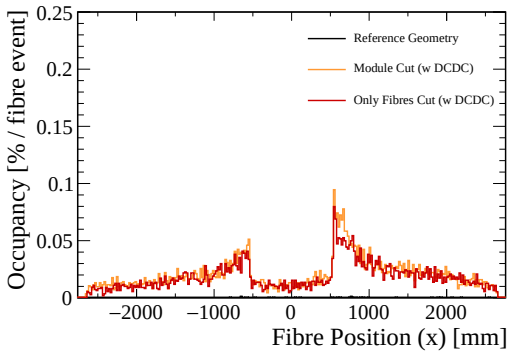

(e) Silicon, Layer 1

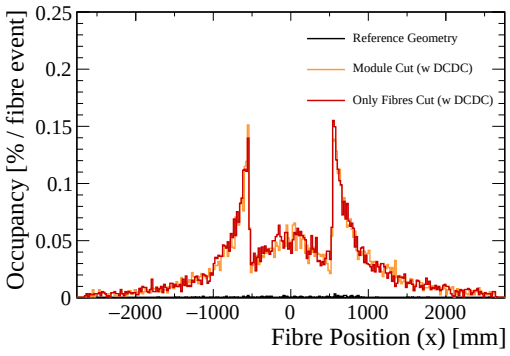

(f) Silicon,Layer 6

Figure 22: Total occupancy in Layer 1 (a) and Layer 6 (b) for the Reference Geometry (black line), the geometry 'Module Cut (with DCDC)' (orange line) and 'Fibres Cut (with DCDC)' (red line). Plots (c) and (d) show the contribution of secondaries from the SciFi stations. Plots (e) and (f) show the contribution from the IT silicon detectors. A group size of 80 fibres is used throughout and the events are simulated with Magnet Up.

The total occupancy is comparable in magnitude between the two options, as seen in plots (a) and (b) of Figure 22. The mean occupancy averaged over all fibres in Layer 1 (Layer 6) is $0.4774 \pm 0.0013\,\%$/fibre.event ($0.6035 \pm 0.0014\,\%$/fibre.event) for the Module Cut and $0.4863 \pm 0.0013\,\%$/fibre.event ($0.6298 \pm 0.0015\,\%$/fibre.event) for the Fibre Cut Geometry. The difference is more easily visible in plots (c) and (d) which show only the occupancy contribution from secondary particles produced in the SciFi stations. Entirely

removing the material of the SciFi module within the xy zone of the IT coverage presents less material for production of secondaries, explaining the lower contribution for the Module Cut Geometry. However, the occupancy here may be an optimistic estimate for this approach to modifying the SciFi, since removing a section of the module housing may necessitate additional support structures (not simulated in this study) which would also produce secondary particles. Plots (e) and (f) show the contribution from the IT layers added for these simulations. Over the whole distribution, there is no statistically significant difference in the magnitude of the contributions from these IT layers.

9.3 Addition of DCDC converters to the IT layer material

As described in Section 3.1, modifications of the geometry and material content of the IT layers are introduced to study the effect of adding or removing DCDC converters in the acceptance of the IT. In Figure 23, the total occupancy in Layers 1 and 6 is shown (plots (a) and (b)), along with the contributions due to the IT layers (plots (c) and (d)) and the cables for the IT (plots (e) and (f)). The higher rate of secondary particle production associated with the additional copper from the DCDC converters significantly increases the occupancy contribution from the IT, as can be seen in plots (c) and (d). The mean contribution from the IT material over all fibres increases from $0.01075 \pm 0.00019\,\%$/fibre.event ($0.01676 \pm 0.00024\,\%$/fibre.event) to $0.01844 \pm 0.00025\,\%$/fibre.event ($0.02710 \pm 0.00030\,\%$/fibre.event) in Layer 1 (Layer 6). Since the IT layers contribute only a small fraction of the total occupancy, the effect is not easily visible in the total occupancy plots in (a) and (b). The thicker cables implemented to compensate for the absence of DCDC converters make a contribution comparable to the IT layers in this geometry scenario for the fibre groups near the edges of the IT at $x = \pm 530\,\text{mm}$. The largest two peaks correspond to the vertical cables, since they run parallel to the fibres. The component of the contribution among the central fibre groups is mostly from the horizontal cables, which are terminated at $x = \pm 100\text{mm}$. The decreased contribution from thinner cables upon the implementation of DCDC converters partially offsets the increased contribution from the IT layers. Nevertheless, the average over all layers and all fibres for the total occupancy still increases from $(0.53817 \pm 0.00055)\,\%$/fibre.event (Fibres Cut w/o DCDC) to $(0.54873 \pm 0.00056)\,\%$/fibre.event(Fibres Cut w DCDC).

9.4 Comparison of geometry scenarios for the Mighty Tracker

The four geometry scenarios for the downstream tracker are compared by studying the average occupancies in the peak fibres and central fibres in each of the SciFi x-layers. The total occupancy in each layer is presented in Figure 24(a) for the average over peak fibre groups and in 24(b) for the average over central fibre groups. Distributions for each of the simulated detector geometries are overlaid.

Occupancies in the peak fibres tend to be much higher (more than a factor two) than in the central fibres. This effect is quantified in Table 11, where averages over the six SciFi x-layers are computed for the occupancies in peak fibres and in central fibres. For the Reference Geometry for example, the average occupancy over all layers in the peak fibres is $\sim 1.2\%$/fibre.event while it is $\sim 0.5\%$/fibre.event in the central fibres. It can be seen that the downstream x-layer of each SciFi station has a significantly higher occupancy than its upstream counterpart for all geometry configurations. The occupancy also increases

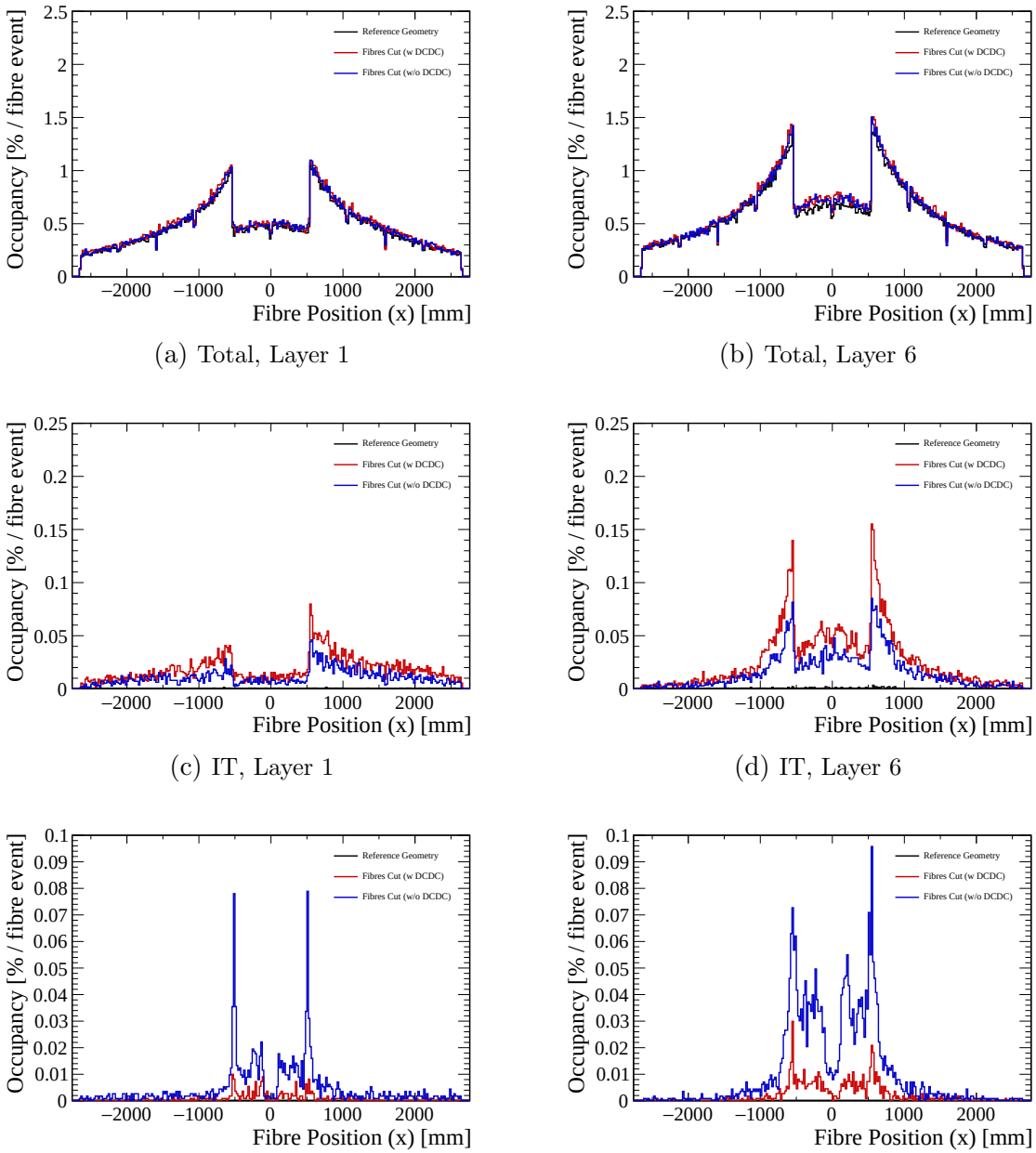

(a) Total, Layer 1

(b) Total, Layer 6

(c) IT, Layer 1

(d) IT, Layer 6

(e) Cables, Layer 1

(f) Cables,Layer 6

Figure 23: Total occupancy in Layer 1 (a) and Layer 6 (b) for the Reference Geometry (black line), the geometry 'Fibres Cut (with DCDC)' (red line), and 'Fibres Cut (without DCDC)' (blue line). Plots (c) and (d) show the contribution of secondaries from the IT layers. Plots (e) and (f) show the contribution of the cables (both the horizontal and vertical sections). A group size of 80 fibres is used throughout and the events are simulated with Magnet Up.

from Layer 1 to Layer 3 and from Layer 3 to Layer 5, which is expected as each of these layers has increasingly more material within their respective acceptance. The same trend is observed for layers 2, 4 and 6. However, total occupancies are lower in Layers 3 than Layer 2, and lower in Layer 5 than Layer 4, indicating that a fraction of the secondary particles produced in a SciFi station are outside of the acceptance of the peak or central

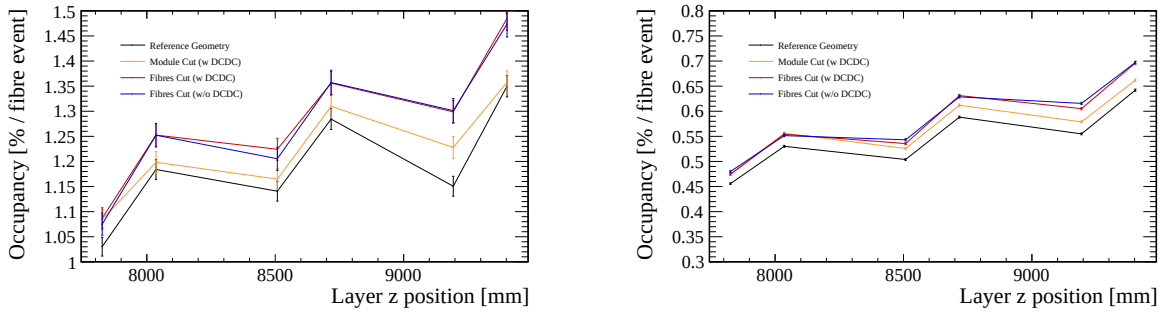

(a) Total Occupancy (Peak fibre groups)

(b) Total Occupancy (Central fibre groups)

Figure 24: Average occupancy over the four peak fibre groups (a) and over the central fibres (b), for events from both magnet polarities, shown at the position of each layer along the z axis, for the Reference Geometry (black), the geometry 'Module Cut (with DCDC)' (orange), 'Fibres cut (with DCDC)' (red) and 'Fibres cut (without DCDC)' (blue). Error bars show the statistical uncertainty. Connecting lines guide the eye.

Table 11: Average over all SciFi x-layers of the occupancies in the peak fibre groups and central fibres groups shown in Fig.24 and 25.

Geometry Scenario	Reference	Module Cut (w DCDC)	Fibres Cut (w DCDC)	Fibres Cut (w/o DCDC)
Peak Fibre Groups				
Av. Occupancy [%/fibre.event] : Total	1.1900(82)	1.2238(86)	1.2840(91)	1.2775(97)
Av. Occupancy [%/fibre.event] : SciFi contribution	0.3097(42)	0.2028(36)	0.2686(42)	0.2731(45)
Av. Occupancy [%/fibre.event] : IT contribution	0.00077(21)	0.1179(27)	0.1098(27)	0.0661(22)
Central Fibre Groups				
Av. Occupancy [%/fibre.event] : Total	0.54583(76)	0.56824(82)	0.58277(84)	0.58600(90)
Av. Occupancy [%/fibre.event] : SciFi contribution	0.17333(43)	0.15349(43)	0.17209(46)	0.17020(48)
Av. Occupancy [%/fibre.event] : IT contribution	0.000294(18)	0.03083(19)	0.02923(19)	0.01830(16)

fibres of the next stations. In terms of total occupancy, either in peak fibres or central fibres, the Reference Geometry displays the lowest values for all layers. The 'Fibres Cut (with DCDC)' and 'Fibres Cut (without DCDC)' configurations are compatible, showing no statistically significant differences in their total occupancies. These geometries have the highest occupancies due to the additional material for the IT implementation and preservation of the module housing for the SciFi in the xy zone of the IT coverage (in contrast to the 'Module Cut' modification of the SciFi tracker). The configuration 'Module Cut (with DCDC)' has occupancy values between that of the Reference Geometry and those with 'Fibres Cut'.

Figure 25 serves as a final summary of the effects discussed in this note. It shows the average event occupancy in the peak fibres only for the secondary particles coming from the IT silicon detector layers (a) and from the SciFi stations (b). Figures 25 (c) and (d) show the occupancies from the same respective origins but in the central fibres. The average over all SciFi x-layers of the occupancies coming from the SciFi and the IT stations are also given in Table 11.

One of the effects highlighted by Figures 25 (a) and (c) is the enhanced production of secondaries in the IT layers as more material is added. For the Reference Geometry,

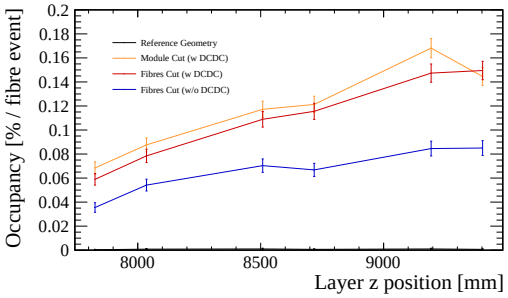

(a) IT Layers (Peak fibre groups)

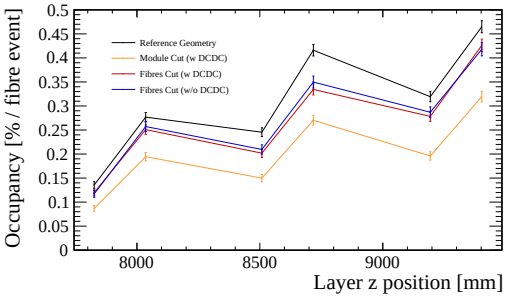

(b) SciFi Stations (Peak fibre groups)

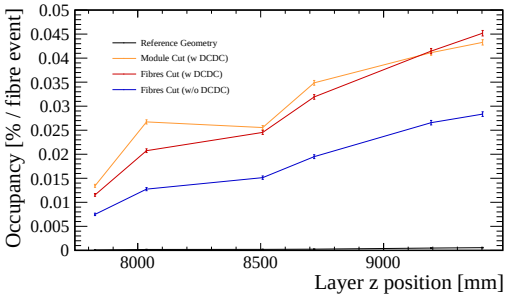

(c) IT Layers (Central fibre groups)

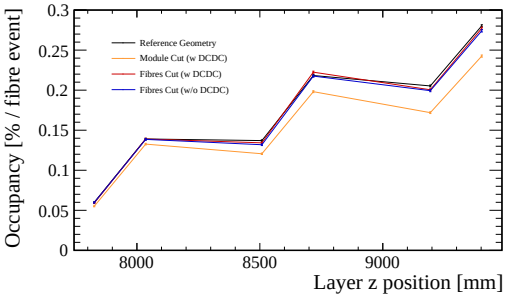

(d) SciFi Stations (Central fibre groups)

Figure 25: Occupancies for the contribution arising from the specified source for the reference geometry (black), the geometry with 'Module cut (with DCDC)' (orange), 'Fibres cut (with DCDC)' (red) and 'Fibres cut (without DCDC)' (blue). Plots (a) and (b) show the average occupancy for the peak fibre groups with highest occupancy at the edges of the IT. Plots (c) and (d) show the average of the occupancy in the central fibres. A group size $B = 80$ fibres was used. The average is evaluated over events with both magnet polarities. Error bars show the statistical uncertainty.

contributions from the IT layer volumes come mainly from interactions with the air, and hence the solid black lines in these two figures take only values very close to 0. The blue lines showing the contributions from all IT layers 'Without DCDC' take much higher values (with an average occupancy in peak fibres over all layers of $\sim 0.07\%$/fibre.event), significantly exceeded by the red and orange lines representing geometry configurations 'With DCDC' (respectively $\sim 0.11\%$/fibre.event and $\sim 0.12\%$/fibre.event). The red lines showing the occupancies for a configuration with 'Fibres Cut' take slightly smaller values than the orange lines for the configuration with 'Modules Cut'. This can be explained by the fact that when only fibres are cut, secondary particles coming from the silicon are stopped by the remaining module housing which surrounds the fibres.

The contributions from the SciFi stations appear in Figures 25 (b) for the occupancy in peak fibre groups and (d) for the occupancy in central fibre groups. Figure 25 (d) in particular shows that the removal of fibres in the central region of the SciFi does not modify significantly the occupancy in central fibre groups, while the removal of the entire module structure helps reduce the occupancy in these fibres. In Figure 25 (c), it can be observed that the occupancy in the peak fibres is more sensitive to the modifications between geometries in the central region. Here, the highest occupancies are obtained for the Reference Geometry (with an average occupancy in peak fibres over all layers

of $\sim 0.31\%$/fibre.event). The blue line below the Reference Geometry corresponds to the configuration 'Fibres Cut (without DCDC)' ($\sim 0.27\%$/fibre.event on average), which is situated just above the red line corresponding to 'Fibres Cut (with DCDC)'. Once more, this trend could be explained by the screening effect due to the presence of the denser material of the IT layer in the presence of DCDC converters in front of the SciFi layers, which reduces the occupancy from secondaries coming from upstream SciFi stations. Finally, the configuration with 'Modules Cut' has once again the lowest values of occupancy coming from the SciFi stations ($\sim 0.20\%$/fibre.event on average in the peak fibres). The reduction of occupancy in the peak fibres between this configuration and the Reference Geometry reaches $\sim 0.1\,\%$/fibre.event on average over all layers. This demonstrates that the SciFi module housing is a significant source of secondary particle production, and this result will inform the decision as to which type of modification of the SciFi is adopted for LS3 enhancements. Since the configuration with 'Module Cut' would likely require some new mechanical support mechanism, the benefits to track reconstruction of any remaining reduction in occupancy would need to be weighed against the additional cost and effort involved in its installation.

9.5 Event-by-event fluctuations

In order to inform the development of new track reconstruction algorithms and data transmission hardware design, the fluctuations in occupancy across different events are studied via the distribution of occupancy calculated for each of the events. This event-by-event occupancy is denoted by $\mathcal{O}_i(x_{\text{group}})$ in Equation 1.

The resolution of the event-by-event occupancy is determined by the group size chosen, in this case $B = 80$ fibres. Accounting for the top and bottom modules gives $2B$ fibres contributing to the specified x interval corresponding to one fibre group. With more hits, the event-by-event occupancy can only increase in steps corresponding to one additional fibre being activated during the same event. This means the smallest step, and hence resolution, of the occupancy is $(1/2B)$/fibre (equivalently $(50/B)\%$/fibre). This puts the resolution of the event-by-event occupancy distribution at 0.625%/fibre for $B = 80$ fibres, and this value will be used as the bin size when plotting event-by-event occupancy distributions.

Event-by-event occupancy distributions in the fibre group of size 80 between $x = 540\,\text{mm}$ and $x = 560\,\text{mm}$ are shown in Figure 26 for Layer 1 (a) and Layer 6 (b). These distributions are very similar for all four geometry scenarios and show a large tail towards higher values of the occupancies.

In order to study the proportion of potentially problematic events with high occupancies, a cumulative representation of the event-by-event occupancy distribution is presented in Figure 27. It is derived from the distributions in Figure 26 by plotting the fraction of events with event-by-event occupancy equal to or greater than the event-by-event occupancy at the lower edge of that bin. The value of that bin is renamed 'Occupancy Threshold' since the bin content is the total fraction found to fall above such a threshold in the simulations considered. This provides an interpretation to inform software development efforts. For example, if the reconstruction efficiency of an algorithm becomes unacceptably poor for occupancy $> 2.5\%$/fibre, the plots show that in Layer 1, $\sim 10 - 15\%$ of events will be in this problematic regime. Layer 6 would present a greater constraint, since the fraction in this regime is $\sim 20 - 25\%$ of events.

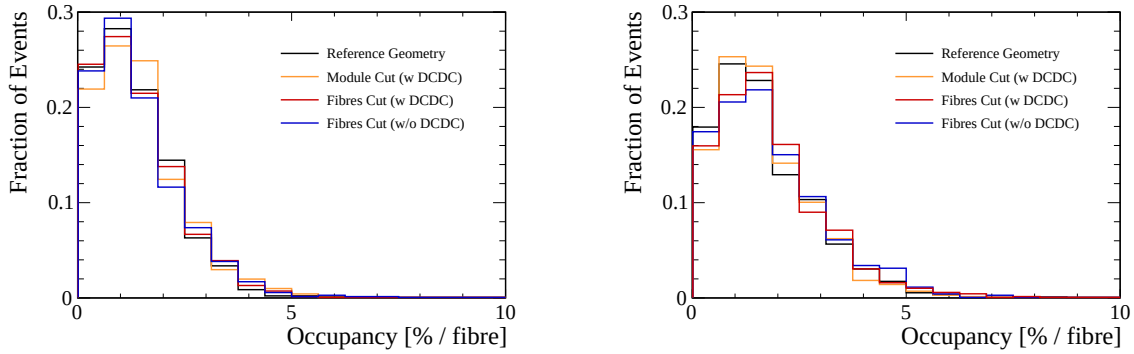

(a) Layer 1 (b) Layer 6

Figure 26: Event-by-event occupancy distributions for the Reference Geometry (black), and the geometries 'Module Cut (with DCDC)' (orange), 'Fibres Cut (with DCDC)' (red) and 'Fibres Cut (without DCDC)' (blue). The bin size is chosen so as to match the resolution in event-by-event occupancy obtained from the choice of group sizes of 80 fibres. The occupancy shown is an average over the top and bottom groups of fibres centred at $x = +550\,\text{mm}$. Events are simulated with Magnet Up.

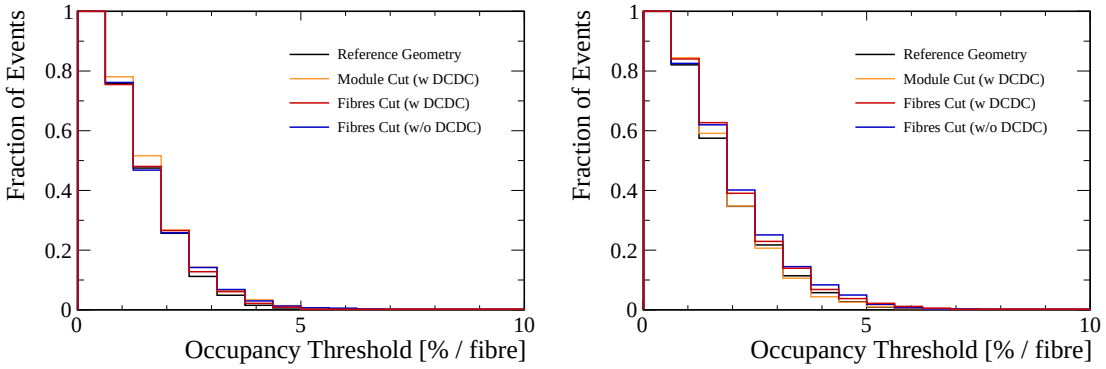

(a) Layer 1 (b) Layer 6

Figure 27: Fraction of events with an event-by-event occupancy equal to or greater than the threshold indicated at the lower edge of each bin, shown for the reference geometry (black), the geometry 'Module Cut (with DCDC)' (orange), 'Fibres Cut (with DCDC)' (red) and 'Fibres Cut (without DCDC)' (blue). A group size $B = 80$ fibres is used, and the occupancy shown is an average over the top and bottom groups of fibres centred at $x = +550\,\text{mm}$. Events are simulated with Magnet Up.

10 Conclusion

A simplified description of materials of an Inner Tracker for LHCb in the LS3 enhancements has been implemented in the GEANT4 description of the LHCb Upgrade I geometry. Expected occupancies in the SciFi have been estimated for different scenarios of the material distribution in the Inner Tracker and the inner modules of the SciFi itself. The contributions to the SciFi occupancy of secondary particles produced in different regions

of the LHC beampipe and the LHCb detector have been studied.

It has been found that the total occupancy is the highest for configurations where the mechanical structure of the SciFi is kept in the central region while only the fibres inside are removed. Removing the mechanical structure of the SciFi lowers the total occupancy in the fibres from 1.28 % per fibre per event to 1.22 % per fibre per event. The two scenarios considered for the IT design (with DCDC converters on the sensitive plane and thinner cables, or without DCDC converters but thicker cables) give rise to similar total occupancies, even if the contribution of the Inner Tracker alone to this occupancy is higher in the presence of DCDC converters.

It should be noted that the present simulation used a simplified description of fibres and did not include any description of the detector response. All occupancy values quoted in this note assume a constant cluster size of one. A simple toy study indicates that it should be possible to obtain a reasonably good estimate of the true occupancy by simply scaling the numbers quoted in this note by the expected cluster size.

In the future, additional studies of occupancy in the SciFi tracker with the LS3 enhancements are envisaged in order to explore more design options (in particular a scenario where the entire SciFi structure is kept, including fibres, alongside the silicon detector planes) and to include the effects of local inhomogeneities in the material composition (*e.g.* due to the presence of power converters on the silicon detector planes).

Appendix

A Secondary particles in the Module Cut geometry

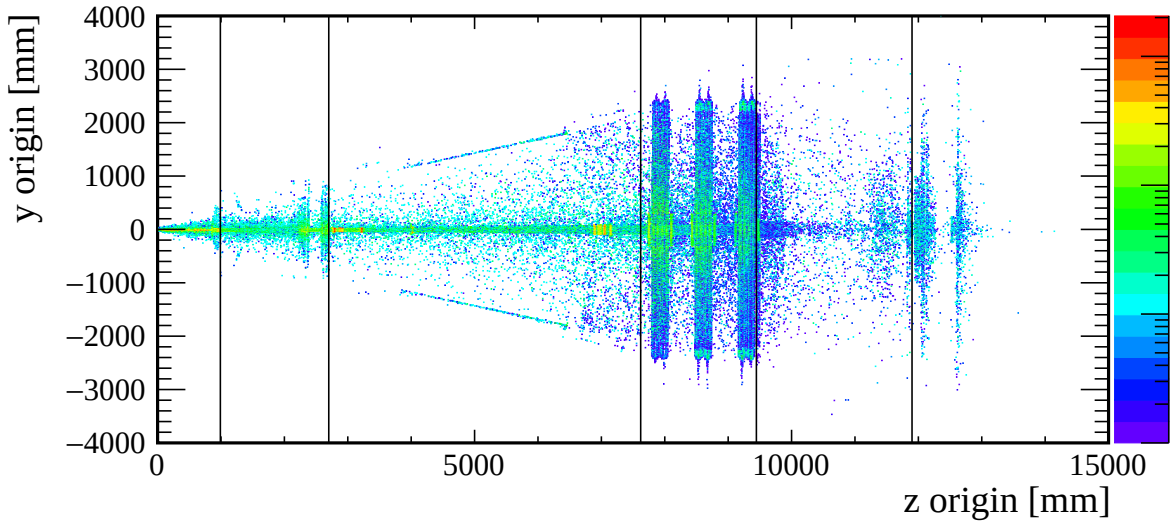

Figure 28: Scatter plot of the (z,y) coordinates of the origins of secondary particles generating hits in the SciFi for the simulation with Module Cut Geometry. Vertical black lines indicate the boundaries separating the six detector regions (R.I-R.VI).

B Origin-distinguished occupancy in different scenarios

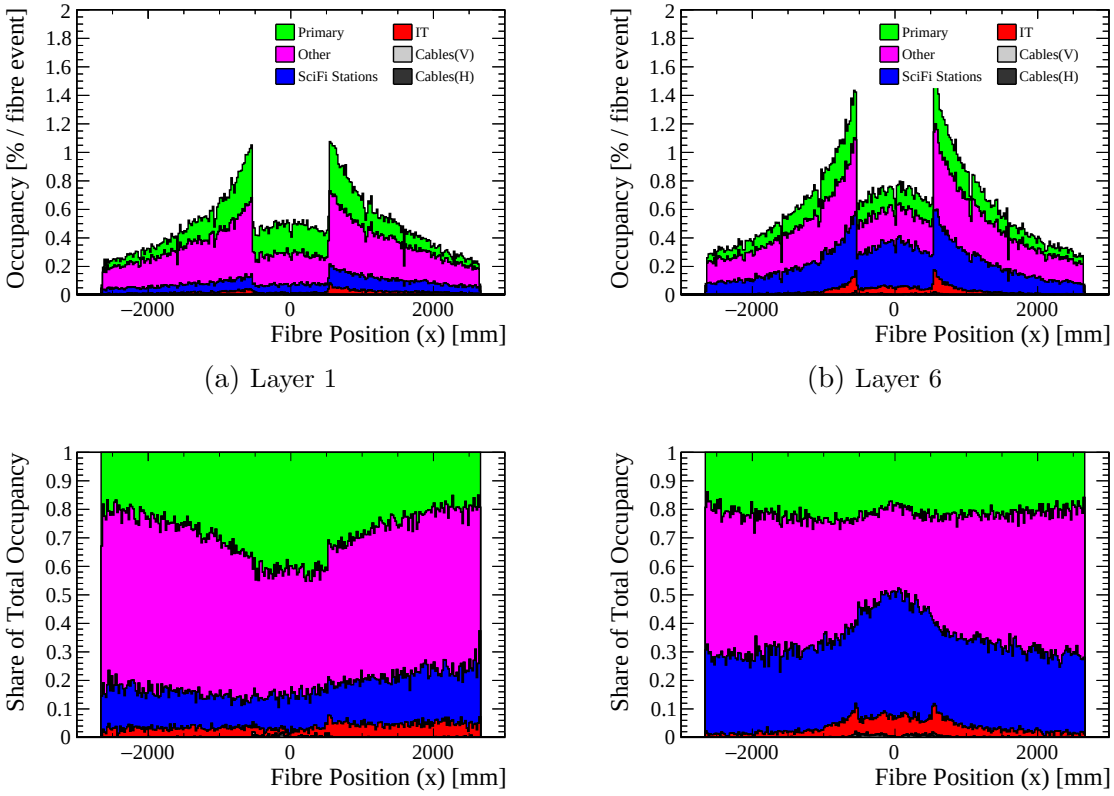

(a) Layer 1

(b) Layer 6

(c) Layer 1

(d) Layer 6

Figure 29: Occupancy and share of the total occupancy for Layers 1 and 6, plotted as a function of the fibre position for the geometry with fibres cut and DCDC converters. The contributions from primary particles (in green) and secondary particles from IT layers (in red), horizontal cables (dark grey), vertical cables (light grey), SciFi stations (in blue) and other sources (in magenta) are stacked. A bin size of 80 fibres is used and events are simulated with Magnet Up.

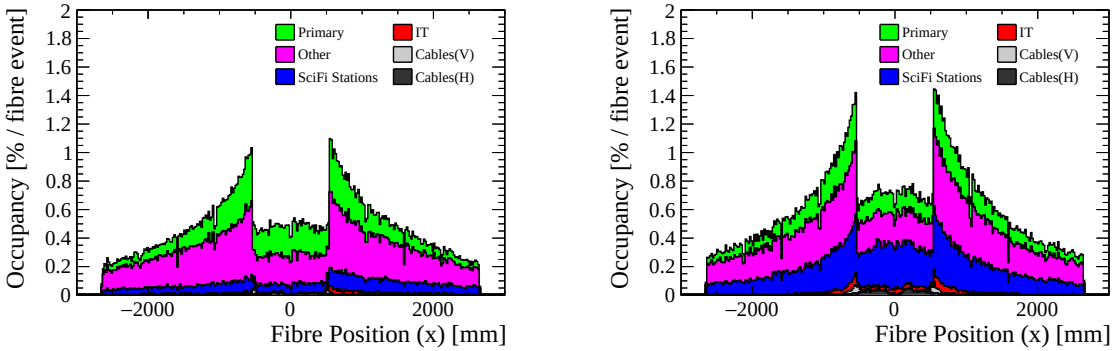

(a) Layer 1

(b) Layer 6

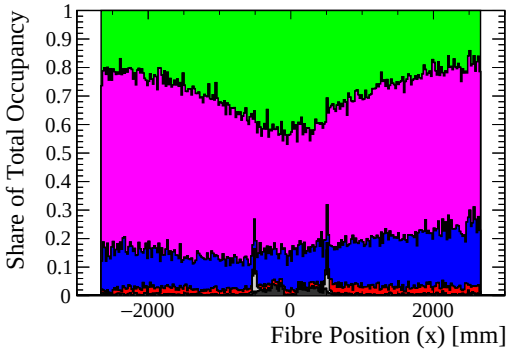

(c) Layer 1

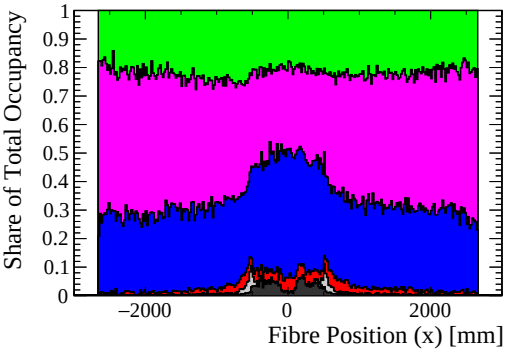

(d) Layer 6

Figure 30: Occupancy and share of the total occupancy for Layers 1 and 6, plotted as a function of the fibre position for the geometry with fibres cut without DCDC converters. The contributions from primary particles (in green) and secondary particles from IT layers (in red), horizontal cables (dark grey), vertical cables (light grey), SciFi stations (in blue) and other sources (in magenta) are stacked. A bin size of 80 fibres is used and events are simulated with Magnet Up.

C Fraction of incoming particles below a momentum threshold

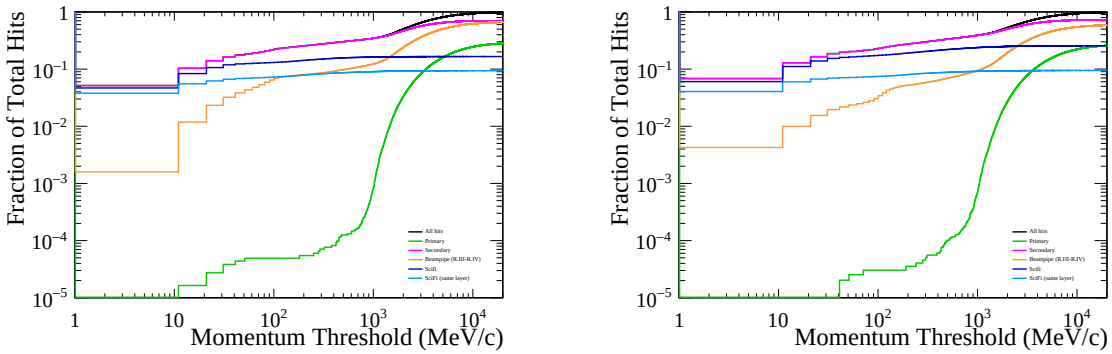

(a) Layer 1

(b) Layer 2

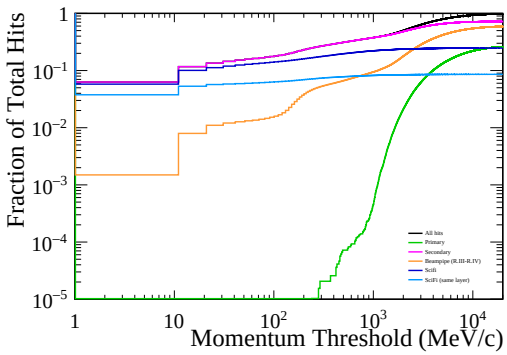

(c) Layer 3

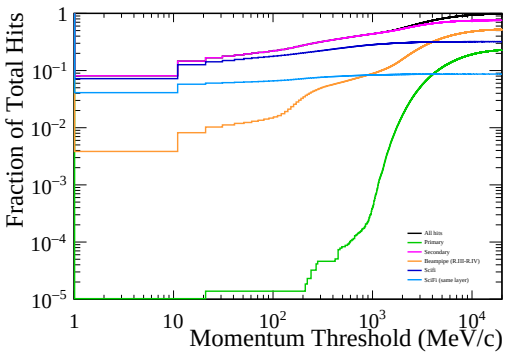

(d) Layer 4

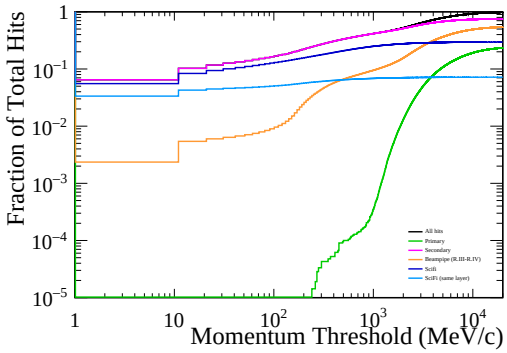

(e) Layer 5

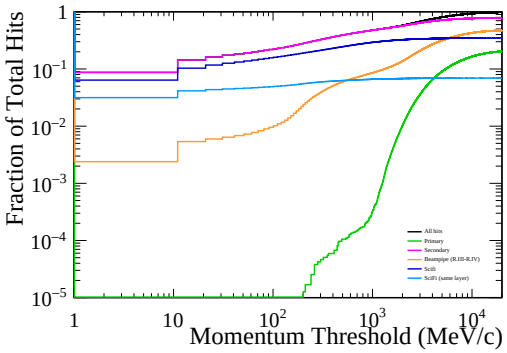

(f) Layer 6

Figure 31: Fraction of hits with a momentum below threshold, separated by origins of the incoming particles responsible for the hits. The graduation on the right of each bin indicates the momentum threshold applied. The contributions shown are from the primary particles (in green) and secondary particles (in pink). Among the secondary particles, a distinction has been made between particles from the beampipe region (in orange), from the SciFi region (in dark blue) and from the same SciFi layer (in light blue). The total of all contributions (in black) reaches the value one at the upper right corner of the plots.

D Origins of backwards moving secondary particles inside the secondary peak of time propagation

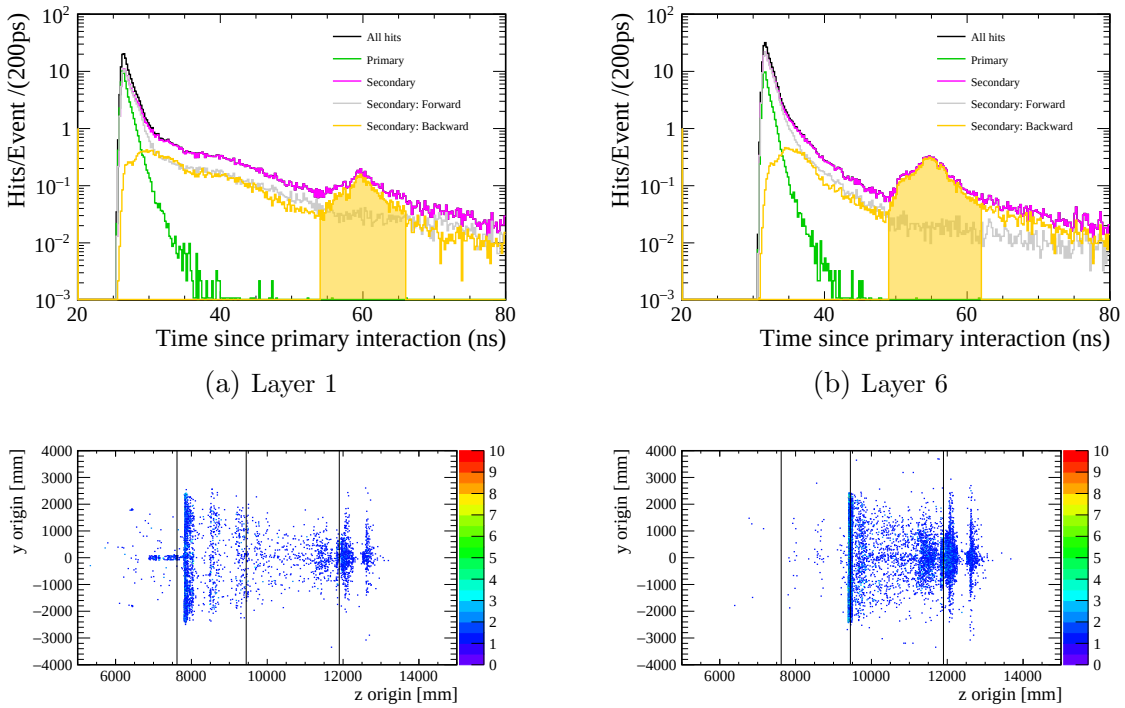

(a) Layer 1

(b) Layer 6

(c) Layer 1

(d) Layer 6

Figure 32: Top: Distributions of the time since the primary interaction for hits in SciFi layer 1 (left) and layer 6 (right), where the contributions of hits from secondary interactions are separated between those coming from particles travelling backwards and forwards. The cuts identifying the secondary peak are shown in the yellow area. Bottom: Scatter plot of the (z, y) coordinates of the origins of the backwards moving secondary particles associated to the secondary peak shown in yellow in the above distributions.

E Beampipe Description

Table 12: The (z, y) coordinates defining the polycones used to approximate the fine structure of the beampipe in Region III are listed for the six volumes implemented. The polycones are volumes of revolution about the z axis generated by the line connecting coordinates 1,2,3 and 4 (in that order). There are five sections of the beampipe in Region III: UX85/1, UX85/C2800 (Compensator 2800), UX85/2, UX85B6900 (Bellows 6900), UX85/3. The flanges connecting these sections, bellows in both UX85/C2800 and UX85/B6900, and the support collars in UX85/2 and UX85/3 are responsible for the intense production of secondaries in the defined volumes. All coordinates in units of mm.

Volume(s)	Coordinate 1	Coordinate 2	Coordinate 3	Coordinate 4
UX85/1 Flange 11 UX85/C2800 Flange 1	$(2744, 30)$	$(2745, 49)$	$(2820, 49)$	$(2821, 31)$
UX85/C Bellows	$(2846, 32)$	$(2847, 40)$	$(2948, 40)$	$(2949, 33)$
UX85/C Flange 12 UX85/2 Flange 1	$(3196, 35)$	$(3197, 49)$	$(3246, 49)$	$(3247, 35)$
UX85/2 Support Collar	$(3977, 42)$	$(3978, 91)$	$(4054, 91)$	$(4055, 43)$
UX85/2 Flange 9 UX85/B6900 UX85/3 Flange 1	$(6872, 71)$	$(6873, 90)$	$(7085, 90)$	$(7086, 74)$
UX85/3 Support Collar	$(7114, 74)$	$(7115, 130)$	$(7175, 130)$	$(7176, 75)$

F Details of the material description for the IT and its cables

F.1 Definition of the IT layer material without DCDC converters

The IT layer material without DCDC converters is described as a homogeneous mixture of the materials in Table 13, with a total density of $0.180\,\mathrm{g/\,cm^3}$.

Table 13: Mixture of materials used to describe a layer of the IT without DCDC converters.

Material	Mass fraction (%)
Silicon	5.1
Kapton	0.3
Carbon foam	11.8
Carbon sheet	19.0
Flex tape	10.7
Epoxy	2.9
PCB	14.1
Armacell	36.2

F.2 Definition of the IT layer material with DCDC converters

The IT layer material with DCDC converters is described as a homogeneous mixture of the materials in Table 14, with a total density of $0.246\,\mathrm{g/cm^3}$.

Table 14: Mixture of materials used to describe a layer of the IT without DCDC converters.

Material	Mass fraction (%)
Silicon	3.4
Kapton	0.2
Carbon foam	7.8
Carbon sheet	12.4
Flex tape	7.0
Epoxy	1.9
PCB	9.2
Armacell	23.7
Copper	12.5
Aluminium	5.2
FR4	8.4

F.3 Kapton

Kapton is defined by its density ($1.420\,\mathrm{g/cm^3}$) and its chemical composition: $C_{22}H_{10}N_2O_5$.

F.4 Carbon foam

The carbon foam is defined as pure carbon with density ($0.200\,\mathrm{g/cm^3}$) and radiation length (185.7 cm).

F.5 Carbon sheet

The carbon foam is defined by its density ($1.720\,\mathrm{g/cm^3}$), its radiation length (23.7 cm) and its chemical composition: $C_9H_6O_2N_3$.

F.6 Flex tape

The flex tape is defined as a mixture of materials with a total density of $1.710\,\mathrm{g/cm^3}$), a radiation length of 9.6 cm and the following mass fractions:

- Kapton: 74.1 %
- Copper: 22.4 %
- HysolBoronNitride: 3.5 %

F.7 HysolBoronNitride

HysolBoronNitride is defined as a mixture of materials with a total density of 1.342 g/ cm^3) and the following mass fractions:

- UT Epoxy: 76.9 %
- BoronNitride: 23.1 %

F.8 UT Epoxy

UT Epoxy is defined as a mixture of materials with a total density of 1.3 g/ cm^3 and the following mass fractions:

- Hydrogen: 7.0 %
- Carbon: 76.0 %
- Oxygen: 17.0 %

F.9 BoronNitride

Boron nitride is defined by its density (2.29 g/ cm^3) and its chemical composition: BN.

F.10 Epoxy

Epoxy is defined by its density (1.2 g/ cm^3), its radiation length (34.9 cm) and its chemical composition: $C_{27}H_{32}O_4N_2$.

F.11 PCB

The PCB material is defined as a mixture of materials with a total density of 2.44 g/ cm^3), a radiation length of 17.0 cm and the following mass fractions:

- UT Epoxy: 4.6 %
- SiO2: 46.7 %
- Copper: 21.0 %
- Stesalite: 27.8 %

F.12 Stesalite

Stesalite is defined as a mixture of materials with a total density of 1.6 g/ cm^3) and the following mass fractions:

- UT Epoxy: 30.0 %
- SiO2: 70.0 %

F.13 SiO2

SiO2 is defined by its density ($2.64\,\mathrm{g/\,cm^3}$) and its chemical composition: SiO_2.

F.14 Armacell

Armacell is defined by its density ($0.08\,\mathrm{g/\,cm^3}$), its radiation length ($801.3\,\mathrm{cm}$) and its chemical composition: C_5H_8.

F.15 Boron

Boron is defined as a mixture of materials with a total density of $2.340\,\mathrm{g/\,cm^3}$) and the following mass fractions:

- Boron 10 (molar mass $A = 10.0\,\mathrm{g/mole}$ and an atomic number $Z = 5$): 20.0 %
- Boron 11 (molar mass $A = 11.0\,\mathrm{g/mole}$ and an atomic number $Z = 5$): 80.0 %

F.16 Silicon

Silicon is defined as a standard material with a density of $2.33\,\mathrm{g/\,cm^3}$, a molar mass of $28.09\,\mathrm{g/mole}$ and an atomic number $Z = 14$.

F.17 Copper

Copper is defined as a standard material with a density of $8.96\,\mathrm{g/\,cm^3}$, a molar mass of $63.546\,\mathrm{g/mole}$ and an atomic number $Z = 29$.

F.18 Aluminium

Copper is defined as a standard material with a density of $2.7\,\mathrm{g/\,cm^3}$, a molar mass of $26.98\,\mathrm{g/mole}$ and an atomic number $Z = 13$.

F.19 Oxygen

Oxygen is defined as a standard material with a density of $0.143 \cdot 10^{-2}\,\mathrm{g/\,cm^3}$, a molar mass of $15.999\,\mathrm{g/mole}$ and an atomic number $Z = 8$.

F.20 Nitrogen

Oxygen is defined as a standard material with a density of $0.125 \cdot 10^{-2}\,\mathrm{g/\,cm^3}$, a molar mass of $14.01\,\mathrm{g/mole}$ and an atomic number $Z = 7$.

F.21 Hydrogen

Hydrogen is defined as a standard material with a density of $0.708 \cdot 10^{-1}\,\mathrm{g/\,cm^3}$, a molar mass of $1.00794\,\mathrm{g/mole}$ and an atomic number $Z = 1$.

References

[1] LHCb collaboration, *Physics case for an LHCb Upgrade II — Opportunities in flavour physics, and beyond, in the HL-LHC era*, arXiv:1808.08865.

[2] LHCb collaboration, *Framework TDR for the LHCb Upgrade: Technical Design Report*, CERN-LHCC-2012-007, 2012.

[3] LHCb collaboration, *LHCb Framework TDR for the LHCb Upgrade II Opportunities in flavour physics, and beyond, in the HL-LHC era*, CERN-LHCC-2021-012, 2022.

[4] LHCb collaboration, R. Aaij *et al.*, *LHCb detector performance*, Int. J. Mod. Phys. **A30** (2015) 1530022, arXiv:1412.6352.

[5] Geant4 collaboration, S. Agostinelli *et al.*, *Geant4: A simulation toolkit*, Nucl. Instrum. Meth. **A506** (2003) 250.

[6] Geant4 collaboration, J. Allison *et al.*, *Geant4 developments and applications*, IEEE Trans. Nucl. Sci. **53** (2006) 270.

[7] LHCb collaboration, *LHCb Tracker Upgrade Technical Design Report*, CERN-LHCC-2014-001, 2014.

[8] V. Denysenko, L. Dufour, L. Grillo, and O. Steinkamp, *Occupancy studies for the Downstream Tracking Stations of LHCb Upgrade Ib and II*, LHCb-INT-2020-020, CERN-LHCb-INT-2020-020, 2020.

[9] *CERN DCDC project*, https://espace.cern.ch/project-DCDC-new/_layouts/15/start.aspx#/. Accessed: 2022-07-13.

[10] D. Murray, *Developing silicon pixel detectors for LHCb: constructing the VELO Upgrade and designing a MAPS-based tracking detector*, CERN-THESIS-2021-325, 2021, Presented 12 Jan 2022.

[11] *DDDB project, version: dddb-20210218*, https://gitlab.cern.ch/lhcb-conddb/DDDB/-/tree/upgrade/dddb-20210218. Accessed: 2022-07-12.

[12] S. Giani *et al.*, *Digitization of SiPM signals for the LHCb Upgrade SciFi tracker*, LHCb-PUB-2014-025, CERN-LHCb-PUB-2014-025, LHCb-INT-2013-065, 2014.